HHS Public Access

Author manuscript

Neuroimage. Author manuscript; available in PMC 2022 October 15.

Published in final edited form as:

Neuroimage. 2022 October 15; 260: 119417. doi:10.1016/j.neuroimage.2022.119417.

Development of high quality T_1-weighted and diffusion tensor templates of the older adult brain in a common space

Yingjuan Wu[a], **Abdur Raquib Ridwan**[a], **Mohammad Rakeen Niaz**[a], **Xiaoxiao Qi**[a], **Shengwei Zhang**[b], **Alzheimer's Disease Neuroimaging Initiative**[c], **David A. Bennett**[b], **Konstantinos Arfanakis**[a,b,*]

[a]Department of Biomedical Engineering, Illinois Institute of Technology, Chicago, IL USA

[b]Rush Alzheimer's Disease Center, Rush University Medical Center, Chicago, Illinois USA

[c]A portion of the data used in preparation of this article were obtained from the Alzheimer's Disease Neuroimaging Initiative (ADNI) database (adni.loni.usc.edu). As such, the investigators within the ADNI contributed to the design and implementation of ADNI and/or provided data but did not participate in analysis or writing of this report. A complete listing of ADNI investigators can be found at: http://adni.loni.usc.edu/wp-content/uploads/how_to_apply/ADNI_Acknowledgement_List.pdf USA

Abstract

High-quality T_1-weighted (T_1w) and diffusion tensor imaging (DTI) brain templates that are representative of the individuals under study enhance the accuracy of template-based neuroimaging investigations, and when they are also located in a common space they facilitate optimal integration of information on brain morphometry and diffusion characteristics. However, such multimodal templates have not been constructed for the brain of older adults. The purpose of this work was threefold: (A) to introduce an iterative method for construction of multimodal T_1w and DTI templates that aims at maximizing the quality of each template separately as well as the spatial matching between templates, (B) to use this method to develop T_1w and DTI templates of the older adult brain in a common space, and (C) to evaluate the performance of the method across iterations and compare it to the performance of state-of-the-art approaches based on multichannel registration. It was demonstrated that more iterations of the proposed method enhanced the characteristics and spatial matching of the resulting T_1w and DTI templates.

*Corresponding author. arfanakis@iit.edu (K. Arfanakis).

Declaration of Competing Interest

The authors have no conflict of interest to report.

Credit authorship contribution statement

Yingjuan Wu: Conceptualization, Formal analysis, Investigation, Methodology, Software, Validation, Visualization, Writing – original draft, Writing – review & editing. **Abdur Raquib Ridwan:** Methodology, Software, Validation, Writing – review & editing. **Mohammad Rakeen Niaz:** Methodology, Software, Validation, Writing – review & editing. **Xiaoxiao Qi:** Methodology. **Shengwei Zhang:** Methodology. **Alzheimer's Disease Neuroimaging Initiative:** Data curation. **David A. Bennett:** Data curation, Funding acquisition, Resources. **Konstantinos Arfanakis:** Conceptualization, Data curation, Formal analysis, Funding acquisition, Investigation, Methodology, Project administration, Resources, Supervision, Validation, Visualization, Writing – original draft, Writing – review & editing.

Supplementary materials

Supplementary material associated with this article can be found, in the online version, at doi:10.1016/j.neuroimage.2022.119417.

The templates of the older adult brain generated by the final iteration of the proposed method provided better delineation of brain structures, higher discriminability between tissues, and higher image sharpness near the cortex compared to templates generated with approaches employing multichannel registration. In addition, the spatial matching between the T_1 w and DTI templates constructed by the proposed method approximated the template alignment achieved with methods employing multichannel registration. Finally, when using the templates generated by the proposed method as references for spatial normalization of older adult T_1 w and DTI data, both the intra-modality inter-subject normalization precision and the inter-modality spatial matching were higher in most metrics than those achieved with templates constructed with other methods. Overall, the present work brought new insights into multimodal template construction, generated much-needed high quality T_1 w and DTI templates of the older adult brain in a common space, and conducted a thorough, quantitative evaluation of available multimodal template construction methods.

Keywords

Brain; Template; Multimodal; T_1 -weighted; Diffusion tensor imaging; Aging

1. Introduction

High-quality T_1 -weighted (T_1 w) and diffusion tensor imaging (DTI) brain templates that are representative of the individuals under study have an important role in neuroimaging investigations (Avants et al., 2010b; Fonov et al., 2011; Joshi et al., 2004; Mazziotta et al., 2001; Zhang and Arfanakis, 2018). When these templates are also located in a common space they form a multimodal set of templates that facilitates optimal integration of information on brain morphometry and diffusion characteristics across individuals (Kochunov et al., 2007; Avants et al., 2010a; Kim et al., 2015; Sasamoto et al., 2014; Sydykova et al., 2007), allows voxel-wise multivariate statistical analyses (Avants et al., 2008a), and provides the foundation for constructing additional structural, functional, and connectivity templates and labels to form a comprehensive digital brain atlas (Toga et al., 2006). To date, several pairs of T_1 w and DTI templates of varying quality and located in the same or approximately the same space have been developed for different age groups (Hsu et al., 2015; Mori et al., 2008; Rohlfing et al., 2010; Zhang et al., 2011). However, no multimodal T_1 w and DTI templates have been constructed exclusively from older adult data. It is well known that due to age-related brain changes, manifested in T_1 w and DTI images as tissue atrophy, enlarged ventricles, widened sulci, lesions, increased mean diffusivity, reduced diffusion anisotropy and other signal changes (Blatter et al., 1995; Cabeen et al., 2017; Courchesne et al., 2000; Dickie et al., 2016; Ge et al., 2002; Good et al., 2001; Liu et al., 2003; Scahill et al., 2003; C. D. Smith et al., 2007; Madden et al., 2004; Pfefferbaum and Sullivan, 2003; Salat et al., 2005; Sullivan et al., 2006, 2010), use of young adult T_1 w and DTI templates in studies of older adults increases spatial mismatch across individuals, and reduces the sensitivity and accuracy of analyses (Fonov et al., 2011; Good et al., 2001; Ridwan et al., 2021; Senjem et al., 2005; Van Hecke et al., 2011; Yoon et al., 2009). There is therefore a need for multimodal T_1 w and DTI templates of the older adult brain.

A number of approaches have been used previously to construct multimodal T_1 w and DTI templates, and these approaches can be grouped into those that construct templates: a) in series e.g. first T_1 w and then DTI, or the opposite, and b) in parallel. In the first category, previous work constructed a T_1 w template from data on multiple individuals and applied the resulting transformations to diffusion tensor-derived data which were then averaged to build corresponding templates (e.g. fractional anisotropy and mean diffusivity templates) (Rohlfing et al., 2010). This approach ensured excellent matching between the resulting T_1 w and DTI templates. However, an important limitation was that the spatial transformations that match T_1 w data across multiple individuals do not ensure optimal matching of DTI data from the same individuals, because in T_1 w images most of the contrast is located at the cortex and subcortical structures and there is limited information to guide registration in the white matter where most of the DTI contrast is located, thereby lowering the quality of the DTI template (Zhang and Arfanakis, 2018). Similarly, other work registered average diffusion-weighted images from multiple individuals to the previously constructed ICBM-152 T_1 w template (Mazziotta et al., 1995) and applied those transformations to the diffusion tensor data, which were then averaged to construct a DTI template in ICBM-152 space (Mori et al., 2008). Again, the main limitation was that spatial matching of DTI data across individuals was not optimized, reducing the quality of the DTI template (Peng et al., 2009). Hsu et al., 2015, recognized this limitation and following T_1 w-based alignment of diffusion imaging data to ICBM-152 space (Mazziotta et al., 1995) and construction of a temporary diffusion spectrum imaging (DSI) template, performed additional DSI-based registrations to improve DSI matching across individuals and generated an improved DSI template. However, one limitation of this approach was that since the DSI-based registrations occurred after the T_1 w registrations had been completed, the space of the final DSI template may have deviated slightly from the space of the T_1 w template. Another limitation was that the two templates were based on data from different groups of people having different characteristics which may have limited the spatial matching across templates, and even in regions with apparently good matching, the combination of T_1 w and DSI characteristics may not be representative of the human brain. In brief, previous work constructing multimodal T_1 w and DTI templates in series was able to either optimize template matching across modalities and template quality for only one modality at the cost of low template quality for the other modality, or to optimize template quality for both modalities separately at the cost of reduced template matching across modalities.

To address the above limitations, multimodal templates can be constructed in parallel using multichannel registration (Arthofer et al., 2021; Avants et al., 2008a; Guimond et al., 2002; Irfanoglu et al., 2016; Lange et al., 2020b; Li and Verma, 2011; Park et al., 2003). Multi-channel registration estimates a joint deformation that aims to optimize inter-subject spatial matching for all modalities, thereby ensuring both high template quality and excellent template matching across modalities. However, although this approach may work well when building multimodal T_1 w and T_2 w templates which have similar features, most of the contrast in T_1 w images is in gray matter while most of the contrast in DTI is in white matter, and therefore T_1 w information may be distracting when attempting to optimize inter-subject matching of DTI features, and the opposite (the severity of this problem also

depends on the registration algorithm). We argue that the requirement for simultaneous optimization of inter-subject spatial matching in both T_1w and DTI data may lead to less precise spatial matching of the features of interest in each modality compared to considering each modality separately, thereby compromising the quality of both templates.

The purpose of this work was threefold: (A) to introduce an iterative method for multimodal T_1w and DTI template construction that aims at maximizing the quality of each template as well as the spatial matching between templates by alternating optimization between modalities and applying all transformations to both modalities, (B) to use this method to develop T_1w and DTI templates of the older adult brain in a common space as part of an ongoing project to develop a comprehensive older adult brain atlas named Multichannel Illinois Institute of Technology & Rush university Aging (MIITRA) atlas, and (C) to evaluate the performance of the method across iterations and compare it to the performance of state-of-the-art approaches based on multichannel registration. The proposed method for multimodal T_1w and DTI template construction uses state-of-the-art single modality registration in data from multiple individuals to maximize the quality of one template and applies the resulting transformations to data from both modalities, then uses single modality registration to maximize the quality of the other template and applies the resulting transformations to data from both modalities, and repeats these steps iteratively, combining the transformations from each step to minimize interpolations. Each iteration aims at maximizing the quality of each of the two templates in series, and multiple iterations aim at enhancing the spatial matching between the two templates. The proposed method was used to develop T_1w and DTI templates of the older adult brain in a common space. The performance of the proposed method was evaluated across iterations and was also compared to that of approaches using multichannel registration in terms of template quality, spatial matching across templates, and spatial normalization of older adult data.

2. Methods

2.1. Participants and data acquisition

Two older adult brain MRI datasets were used in this work. Dataset 1 was used for constructing multimodal T_1w and DTI templates. Dataset 1 consisted of structural T_1w and diffusion data from 202 non-demented older adults (50% male; 65.2–94.9 years age range; mean±sd age=80.56±8.14 years of age; 161 with no cognitive impairment and 41 with mild cognitive impairment) participating in the Rush Memory and Aging Project (MAP) (Bennett et al., 2018). All participants provided written informed consent according to procedures approved by the institutional committee for the protection of human subjects. Previous work has shown that this number of participants is sufficiently large to generate an unbiased and robust brain template (Ridwan et al., 2021; Yang et al., 2020). All data were collected on a 3T Siemens (158 persons) and a 3T Philips MRI scanner (44 persons). T_1w images were acquired using a 3D magnetization prepared rapid acquisition gradient echo (MPRAGE) sequence with the following parameters: for 3T Siemens, TR=2300 ms, TE=2.98 ms, TI=900 ms, flip-angle=9°, field of view=256 mm x 256 mm, 176 sagittal slices, acquired voxel size=$1 \times 1 \times 1$ mm^3, and an acceleration factor of 2; for 3T Philips, TR=8 ms, TE=3.7 ms, TI=955 ms, flip-angle=8°, field of view=240 mm x 228 mm, 181

sagittal slices, acquired voxel size=1 × 1 × 1 mm^3 , and an acceleration factor of 2. The diffusion data were acquired using a spin-echo-planar diffusion-weighted imaging sequence with the following parameters: for 3T Siemens, TR=8100 ms, TE=85 ms, field of view=224 mm x 224 mm, 65 axial slices, voxel size=2 × 2 × 2 mm^3 , b = 1000s/mm^2 for 40 diffusion directions, and six b = 0 s/mm^2 images; for 3T Philips, TR=10,701 ms, TE=55 ms, and all other parameters were the same.

Dataset 2 was used for assessing spatial normalization precision when using the templates generated by the different methods as reference. Dataset 2 consisted of T_1 w and DTI data from 202 non-demented older adults (50% male; 65–93.2 years age range; mean±sd age=78.3±6.02 years of age; 122 with no cognitive impairment and 80 with mild cognitive impairment) participating in the Alzheimer's Disease Neuroimaging Initiative 3 (ADNI3) (http://adni.loni.usc.edu). ADNI was launched as a public-private partnership in 2003, led by Principal Investigator Michael W. Weiner, MD. The primary goal of ADNI has been to test whether serial MRI, positron emission tomography (PET), other biological markers, and clinical and neuropsychological assessment can be combined to measure the progression of mild cognitive impairment and early Alzheimer's disease. All data in Dataset 2 were collected on 3T Siemens (146 persons) and 3T Philips (56 persons) MRI scanners. T_1 w images were obtained using 3D MPRAGE sequences with the following parameters: for 3T Siemens, TR=2300 ms, TE=2.98 ms, TI=900 ms, flip-angle=9°, field of view=256 mm x 240 mm, 208 slices, acquired voxel size=1 × 1 × 1 mm^3 , and an acceleration factor of 2; for 3T Philips, TR=6.5 ms, TE=2.9 ms, TI=900 ms, flip-angle=9°, field of view=256 mm x 256 mm, 211 slices, acquired voxel size=1 × 1 × 1 mm^3 , and an acceleration factor of 2. DTI data were acquired using spin-echo-planar diffusion-weighted sequences with the following parameters: for Siemens Skyra E11 (101 persons), TR=9600 ms, TE=82.0 ms, field of view=232 mm x 232 mm, 80 axial slices, voxel size =2 × 2 × 2 mm^3 , b = 1000s/mm^2 for 48 diffusion directions, and seven b = 0 s/mm^2 images; for Siemens 20VB17 (45 persons): TR= 12,400 ms, TE=95 ms, field of view=232 mm x 232 mm, 80 axial slices, voxel size=2 × 2 × 2 mm^3 , b = 1000s/mm^2 for 30 diffusion directions and one b = 0 s/mm^2 image; for Philips (56 persons), TR=9916 ms, TE=86 ms, field of view=256 mm x256 mm, 80 axial slices, voxel size=2 × 2 × 2 mm^3 , b = 1000s/mm^2 for 32 diffusion directions, and 9 b = 0 s/mm^2 images.

2.2. Image processing

T_1 w images in Datasets 1 and 2 were skull-stripped using a multi-atlas skull-stripping method with a set of 100 atlases (Doshi et al., 2013; Heckemann et al., 2015). The brain images were segmented into white matter, gray matter, and cerebrospinal fluid using CAT12 (Farokhian et al., 2017), and the three masks were used as priors for N4 bias field inhomogeneity correction (Tustison et al., 2010). The resulting image intensities were normalized with z-score normalization using the mean and standard deviation of the intensities inside the combined gray and white matter masks. The gray matter in the T_1 w images of Dataset 2 were also segmented into the Desikan-Killiany regions using FreeSurfer (Fischl, 2012; McCarthy et al., 2015).

Diffusion-weighted images in both Datasets 1 and 2 were corrected for motion, eddy-currents and EPI distortions, and the B-matrix was re-oriented using the DIFFPREP tool of TORTOISE (Irfanoglu et al., 2017; Pierpaoli et al., 2010; Rohde et al., 2004). The diffusion tensors were then estimated in each brain voxel using the DIFFCALC tool of TORTOISE and the RESTORE nonlinear fitting option (Chang et al., 2005, 2012). FA maps were generated from the diffusion tensors.

Prior to template construction, two preprocessing steps were performed for every participant i ($i = 1 \ldots N$, $N = 202$) in Dataset 1. First, the diffusion tensors of participant i, denoted as DTI_i, were registered to that participant's T_1 w data, denoted as T_{1i}, to correct any motion occurring between sequences. To accomplish that, the corrected images with no diffusion weighting, b_{0i}, were affinely registered to T_{1i} using ANTs (Avants et al., 2009, 2011) (affine registration was preferred over rigid body registration because in some cases the former was shown to provide slightly better alignment of DTI and T_1 w data than the latter) with mutual information as the cost function, and the resulting transformation $\varphi_{b_{0i} \to T_{1i}}$ was applied to DTI_i. Next, the T_{1i} data were aligned with MNI space through a rigid transform $\varphi_{T_{1i} \to MNI}$. The DTI_i data were also transformed to MNI space using the combination of the two transforms, $\varphi_{b_{0i} \to T_{1i}} \circ \varphi_{T_{1i} \to MNI}$, to minimize interpolations. The co-registered and MNI-aligned T_1 w and DTI data of Dataset 1 were used in template construction as described next.

2.3. Proposed method for constructing multimodal T_1 w and DTI templates

The proposed method performs spatial normalization across participants based on T_1 w or on DTI data in an alternating fashion, applies all transformations to data from both modalities, and repeats this process for multiple iterations. More specifically, each iteration includes two steps (Fig. 1). In step 1, spatial normalization is driven by T_1 w information, a T_1 w template is generated, and the resulting transformations are also applied to the DTI data (a DTI template is not generated in this step). In step 2, spatial normalization is driven by DTI information that has already been spatially transformed in step 1, a DTI template is generated, and the resulting transformations are also applied to the T_1 w data (a T_1 w template is not generated in this step). Steps 1 and 2 are then repeated for multiple iterations, and the transformations from all steps and iterations are combined so that each image is interpolated only once throughout the whole process. Overall, a) each iteration aims at maximizing the quality of each of the two templates separately, recognizing that data from the two modalities contain very different features, and b) multiple iterations in which the same transformations are applied to both modalities aim to enhance the spatial matching between the two templates. The proposed approach is described in more detail below.

In step 1, T_1 w-based inter-subject spatial normalization was performed according to the procedure outlined by Ridwan et al. (2021) which uses the symmetric group-wise normalization (SyGN) method (Avants et al., 2010b) (Fig. 1). Mutual information and cross-correlation were used as the cost functions for linear and deformable registration respectively (Ridwan et al., 2021; Niaz et al., 2022). The resulting rigid, affine, and non-linear transformations for participant i were concatenated into a single transform $\varphi^1_{T_{1i}}$

(superscript 1 indicates the first iteration), and the combined transform ($\varphi_{T_{1i}\rightarrow MNI}\circ\varphi^{1}_{T_{1i}}$) was applied to the raw T_{1i} data to bring them to common space with a single interpolation. A T_1 w template was then generated from the spatially normalized data using weighted averaging where the weight, $w_i(x)$, for participant i in voxel x was given by a Gaussian kernel (Niaz et al., 2022):

$$w_i(x) = \frac{1}{\sigma(x)\sqrt{2\pi}} e^{-\frac{(S_i(x) - med(x))^2}{2\sigma(x)^2}}, \quad (1)$$

where $S_i(x)$ is the signal of participant i at voxel x and $med(x)$ and $\sigma(x)$ are the median and standard deviation of the population at voxel x. This weighted averaging is based on the widely used kappa-sigma clipping average method (Jörsäter, 1993; Lalys et al., 2010) and helps reduce the effects of residual misregistration on the template. The combined transform $\varphi_{b_{0i}\rightarrow T_{1i}}\circ\varphi_{T_{1i}\rightarrow MNI}\circ\varphi^{1}_{T_{1i}}$ was then applied to the DTI_i data to bring them to common space with a single interpolation, and the results were used in step 2 (Fig. 1).

In step 2, DTI-based inter-subject spatial normalization was performed using the non-linear registration component of DR-TAMAS (dtireg_create_template.sh) (Irfanoglu et al., 2016) on the DTI data that were already transformed in step 1 (Fig. 1). Both deviatoric tensor similarity (Zhang et al., 2007) and trace similarity metrics were used in the cost function (Irfanoglu et al., 2016). The resulting transformation for participant i in step 2, iteration 1, was denoted as $\varphi^{1}_{DTI_i}$. This was concatenated with previous transforms and the combined transform, $\varphi_{b_{0i}\rightarrow T_{1i}}\circ\varphi_{T_{1i}\rightarrow MNI}\circ\varphi^{1}_{T_{1i}}\circ\varphi^{1}_{DTI_i}$ was applied to the DTI_i data to bring them to the new common space with a single interpolation. A DTI template was generated from the spatially normalized data using weighted averaging of the diffusion tensors across participants following the DR-TAMAS formula for the weights (Irfanoglu et al., 2016 Appendix A.4.). Next, the combined transform $\varphi_{T_{1i}\rightarrow MNI}\circ\varphi^{1}_{T_{1i}}\circ\varphi^{1}_{DTI_i}$ was applied to the raw T_{1i} data and the results were used in step 1 of the next iteration (Fig. 1).

Steps 1 and 2 were repeated in multiple iterations, M, until the Pearson cross-correlation similarity index (PCC) across homologous templates from successive iterations was higher than 0.999 (for both T_1 w and DTI templates) (Fig. 1). In the last iteration, the combined transform:

$$\varphi^{total}_{T_{1i}} = \varphi_{T_{1i}\rightarrow MNI}\circ\varphi^{1}_{T_{1i}}\circ\varphi^{1}_{DTI_i}\circ\ldots\circ\varphi^{M-1}_{T_{1i}}\circ\varphi^{M-1}_{DTI_i}\circ\varphi^{M}_{T_{1i}}, \quad (2)$$

was applied to the raw T_{1i} data to bring them to the final space with a single interpolation, and a final T_1 w template was constructed with weighted averaging of signals across participants. Skull and other head structures were added to the final T_1 w template using the strategy by Rohlfing et al. (Rohlfing et al., 2012; Ridwan et al., 2021; Niaz et al., 2022). However, the brain-only template was considered in the rest of this work. The DTI_i data were also brought to the final space with a single interpolation using the combined transform:

$$\varphi_{DT\ I_i}^{total} = \varphi_{b0_i \to T1_i} \circ \varphi_{T1_i \to MNI} \circ \varphi_{T1_i}^{1} \circ \varphi_{DT\ I_i}^{1} \circ \ldots \circ \varphi_{T1_i}^{M-1} \circ \varphi_{DT\ I_i}^{M-1} \circ \varphi_{T1_i}^{M} \circ \varphi_{DT\ I_i}^{M}, \quad (3)$$

and a final DTI template was constructed with weighted averaging of the diffusion tensors across participants. It should be noted here that in the final iteration, M, the DTI_i data experience the transformation $\varphi_{DT\ I_i}^{M}$ which is not applied to the $T1_i$ data (see Eqs. (2) and 3). We argue that after a few iterations where all transformations are applied to both modalities, any misalignment between templates introduced by this final transformation is negligible.

2.4. Evaluation of the proposed method across iterations

To investigate the role of multiple iterations in the proposed method, we evaluated in each iteration a) the precision of spatial normalization across data used for template construction, b) the characteristics of the templates, and c) the spatial matching between the T_1 w and DTI templates.

The precision of spatial normalization of T_1 w data from Dataset 1 was assessed in each iteration by means of the pairwise normalized cross-correlation (PNCC) (Ferreira et al., 2014; Wang et al., 2004):

$$PNCC_{ij} = \frac{1}{N} \times \frac{\sum_{x=1}^{N} (S_i(x) - \mu_i) \times (S_j(x) - \mu_j)}{\sigma_i \times \sigma_j}, \quad (4)$$

where $S_i(x)$ and $S_j(x)$ are the signals of participants i and j at voxel x, μ_i, σ_i and μ_j, σ_j are the mean and standard deviation of the intensities of all the voxels of subjects i and j, and N is the total number of voxels. The average PNCC over all pairs of spatially normalized T_1 w images of Dataset 1 (202×201/2 = 20,301 pairs) was compared across iterations using one-way ANOVA followed by the Tukey-Kramer post-hoc test. Differences were considered significant at $p<0.05$.

The precision of spatial normalization of DTI data from Dataset 1 was assessed in each iteration by means of the pairwise Euclidean distance of tensors (DTED) (Alexander and Gee, 2000; Zhang et al., 2011; Wang et al., 2021):

$$DTED = \sqrt{trace((\boldsymbol{D_i} - \boldsymbol{D_j})^2)}, \quad (5)$$

where $\boldsymbol{D_i}$ and $\boldsymbol{D_j}$ are diffusion tensors of participants i and j in the same voxel. The average DTED over all pairs of spatially normalized DTI data of Dataset 1 (202×201/2 = 20,301 pairs) was calculated in each voxel, and cumulative distributions of the average DTED in white matter (white matter was defined through K-means clustering of mean FA maps) were compared across iterations using the one-sided two-sample Kolmogorov-Smirnov (KS) test. Differences were considered significant at $p<0.05$.

According to the proposed method, T_1 w and DTI data from individual participants undergo the same spatial transformations in all iterations other than the last. Therefore, we assessed the final spatial matching between T_1 w and DTI data of Dataset 1 when terminating the proposed method at different iterations. For that purpose, the white matter mask of participant i (generated in Section 2.2) was transformed to both the final T_1 w space and the final DTI space using the transformations φ_{T1i}^{total} (Eq.2) and $\varphi_{T1t}^{total} \circ \varphi_{DT\ I_i}^{M}$, respectively, and the overlap between the two versions of the white matter mask was assessed using the Jaccard index (JI):

$$J\ I_i = \frac{M_i \cap N_i}{M_i \cup N_i}, \tag{6}$$

where $M_i \cap N_i$ and $M_i \cup N_i$ are the intersection and union of the two versions of the white matter mask of subject i. The average JI over all participants of Dataset 1 was compared across iterations using one-way ANOVA followed by the Tukey-Kramer post-hoc test. Differences were considered significant at $p<0.05$.

The T_1 w templates generated at different iterations were compared visually as well as quantitatively in terms of tissue contrast and image sharpness. Tissue contrast was assessed by means of the Fisher score (FS) (Duda et al., 2012; Misaki et al., 2015):

$$F\ S = \frac{\mu_{W\ M} - \mu_{GM}}{\sqrt{\sigma_{W\ M}^2 + \sigma_{GM}^2}}, \tag{7}$$

where μ_{WM}, σ_{WM} and μ_{GM}, σ_{GM} are the mean and standard deviation of signals in white matter and gray matter voxels. To define which voxels of a template belonged to white or gray matter, tissue masks of the individual participants (generated in Section 2.2) were transformed to template space and were combined using the same transformations and weights applied to the corresponding T_1 w data for template construction, and tissue probability maps were generated in template space and then thresholded to produce white and gray matter masks. The FS between gray matter and cerebrospinal fluid was also calculated following the same approach. Additionally, the sharpness of the T_1 w templates from different iterations was assessed by means of the normalized power spectra along the inferior-superior (IS), left-right (LR) and anterior-posterior (AP) axes separately (Zhang et al., 2011; Ridwan et al., 2021; Niaz et al., 2022).

The DTI templates generated at different iterations were compared visually as well as quantitatively in terms of fractional anisotropy (FA) values in white matter and sharpness of FA maps. Template FA values were projected onto the white matter skeleton (S. M. Smith et al., 2006; Keihaninejad et al., 2012) of the IIT Human Brain Atlas (v.5.0) (Zhang and Arfanakis, 2018) and cumulative distributions of white matter FA values were compared across iterations using the one-sided two-sample Kolmogorov-Smirnov (KS) test (differences were considered significant at $p<0.05$). The sharpness of FA templates from

different iterations was assessed by means of the normalized power spectra along the IS, LR and AP axes separately (Zhang and Arfanakis, 2018; Zhang et al., 2011).

The spatial matching between the T_1w and DTI templates generated at different iterations was evaluated by visual inspection and also quantitatively by means of the overlap of white matter masks and the overlap of gray matter masks corresponding to the T_1w and DTI templates. More specifically, white matter masks of the individual participants (generated in Section 2.2) were transformed to T_1w template space and DTI template space and were combined into white matter probability maps using the same spatial transformations and the same weights applied to the corresponding T_1w and DTI data for template construction. The white matter probability maps of the T_1w and DTI templates were then thresholded to generate corresponding white matter masks and the overlap between the two white matter masks was assessed using the Jaccard index (Eq.6). The same approach was used to assess the overlap of gray matter masks corresponding to the T_1w and DTI templates.

2.5. Comparison of the proposed method to other multimodal template construction methods

The performance of the proposed method for multimodal T_1w and DTI template construction was compared to that of three approaches that employ multichannel registration. The first one, based on T_1w and full tensor information, is available in DR-TAMAS (dtireg_create_template_with_structurals) (Irfanoglu et al., 2016), and will be referred to as MC-DRTAMAS. MC-DRTAMAS uses tensor deviatoric similarity and tensor trace similarity metrics to guide tensor registration and a cross-correlation metric for T_1w registration, generates separate displacement fields for each metric, assigns weights to the different displacements and combines them. The weights used here were: 1 for tensor deviatoric similarity, 1 for tensor trace similarity, and 2 for T_1w cross correlation, so that the overall weights for the two modalities were equal. The second one, based on T_1w and FA information, is available in ANTs (antsMultivariateTemplateConstruction.sh) (Avants et al., 2011) and will be referred to as MC-ANTS. MC-ANTS uses mutual information as the cost function for rigid and affine registration and cross-correlation for deformable registration in both channels. The third one, based on T_1w and full tensor information, utilizes the MMORF tool (run_template_construction.py) (Lange et al., 2020a; https://git.fmrib.ox.ac.uk/cart/mm-template-construction) and will be referred to as MC-MMORF. MC-MMORF uses cubic B-spline elastic transformation with mean squared error as the cost function for T_1w registration and mean squared Frobenius norm for DTI registration, and uses log-Euclidean averaging to generate the DTI template (Lange et al., 2020b; Roumazeilles et al., 2021). MC-DRTAMAS, MC-ANTS and MC-MMORF were applied to the co-registered and MNI-aligned T_1w and DTI data of Dataset 1 (Section 2.2) to generate multimodal T_1w and DTI templates. Transformations were combined to minimize interpolations as in the proposed method. The templates generated by the proposed method were compared to those constructed by MC-DRTAMAS, MC-ANTS and MC-MMORF in terms of a) template characteristics, b) spatial matching between T_1w and DTI templates, and c) intra-modality and inter-modality spatial normalization precision when used as references for spatial normalization of external older adult data.

The T_1w and DTI templates generated with the different methods were compared by visual inspection as well as quantitatively. More specifically, T_1w templates were compared in terms of tissue contrast, image sharpness and standard deviation (calculated across the spatially normalized images used in the construction of the templates), and DTI templates were compared in terms of FA values in white matter, sharpness of FA maps and standard deviation, using the methods described in Section 2.4. The spatial matching between T_1w and DTI templates was compared quantitatively by means of the overlap of white matter masks and the overlap of gray matter masks (as in Section 2.4), as well as by visual inspection of the overlay of the white-gray matter interface defined in T_1w templates on the corresponding FA templates.

The performance of T_1w and DTI templates when used as references for spatial normalization of data from Dataset 2 was compared across multimodal template construction methods by assessing the intra-modality and inter-modality spatial normalization precision. More specifically, T_1w and DTI data from Dataset 2 were registered to each T_1w template using ANTs and to each DTI template using DR-TAMAS, respectively. Symmetric normalization (SyN) diffeomorphic transformation (Avants et al., 2008b) was applied in all ANTs and DR-TAMAS registrations (Klein et al., 2009). To compare the intra-modality inter-subject spatial normalization precision across T_1w templates, the resulting T_1w-based transformations were applied to the corresponding gray matter masks of Dataset 2 and the average pairwise JI over all participants ($202\times201/2 = 20{,}301$ pairs) was compared across templates using one-way ANOVA followed by the Tukey-Kramer post-hoc test. To compare the intra-modality inter-subject spatial normalization precision across DTI templates, the average DTED over all pairs of spatially normalized DTI data of Dataset 2 ($202\times201/2 = 20{,}301$ pairs) was calculated in each voxel, and cumulative distributions of the average DTED in white matter (defined through K-means clustering of FA templates) were compared across templates using the one-sided two-sample Kolmogorov-Smirnov (KS) test. To compare the inter-modality spatial matching across template construction methods, the white matter, gray matter and cerebrospinal fluid masks of participants from Dataset 2 were transformed to both the T_1w template space (using the T_1w-based transformations) and the DTI template space (using the tensor-based transformations) and the average JI between the two versions of the masks over all participants of Dataset 2 was compared across template construction methods using one-way ANOVA followed by the Tukey-Kramer post-hoc test. Differences were considered significant at $p<0.05$.

3. Results

3.1. Evaluation of the proposed method across iterations

With more iterations of the proposed method, the average PNCC over all pairs of spatially normalized T_1w images of Dataset 1 increased ($p<0.05$ in all cases) (Fig. 2A), the standard deviation of PNCC decreased, and the relative number of white matter voxels with low DTED increased ($p<10^{-10}$) (Fig. 2B), indicating improving spatial matching of the T_1w and DTI data used in template construction. In addition, the average JI between WM masks transformed by T_1w and DTI transformations increased with more iterations ($p<10^{-10}$

between iterations 1 and 2), indicating an improving inter-modality matching (Fig. 2C). The amount of improvement decreased with more iterations (Fig. 2). T_1w templates generated with more iterations showed a clearer delineation of brain structures (Fig. 3A) and higher discriminability between tissues (Fig. 3B), particularly near the cortex. The average energy in the normalized power spectra was similar across iterations for all axes (Fig. 3C), indicating similar image sharpness in the T_1w templates across iterations. DTI templates generated with more iterations had FA maps that, near the cortex, provided better delineation of white matter structures (Fig. 4A), had higher image sharpness (Fig. 4B) and higher FA values in a relatively higher number of white matter voxels ($p<10^{-10}$ when comparing iterations 1 and 4) (Fig. 4C). There were no significant differences in the subcortical area of DTI templates across iterations (Fig. 4D,E). The contours of white matter features seen in the FA maps of DTI templates highly conformed to the gyral-sulcal patterns and subcortical features of the T_1w templates according to visual inspection, indicating good spatial matching between T_1w and DTI templates (Fig. 5A). Furthermore, the overlap of tissue masks corresponding to the T_1w and DTI templates as quantified by the Jaccard index increased for more iterations and reached a value of JI=0.966 for white matter overlap and JI=0.95 for gray matter overlap after 4 iterations, where JI=1 is the maximum. The iterative process of the proposed method converged at 4 iterations. The final templates (Fig. 6) are available for download at www.nitrc.org/projects/miitra (version 1.5).

3.2. Comparison of the proposed method to other multimodal template construction methods

The T_1w and DTI templates generated from Dataset 1 using the different methods were compared by visual inspection as well as quantitatively. Features in the cortex, in subcortical structures (e.g. caudolenticular gray bridges), and in the cerebellum were better delineated in the T_1w template generated by the proposed method compared to other methods (Fig. 7A). The standard deviation of the T_1w template generated by the proposed method was lower than that of other methods, especially near the cortex (Fig. 7B). The discriminability between tissues measured by the Fisher score was higher in the T_1w template constructed by the proposed method near the cortex (Fig. 7C) as well as in the subcortical area between gray and white matter (Fig. 7D). The discriminability between gray matter and cerebrospinal fluid in the subcortical area was higher in the T_1w template built with MC-MMORF (Fig. 7D). In addition, the T_1w template of the proposed method exhibited higher energy in the normalized power spectra for all axes near the cortex (Fig. 7E), while the T_1w template of MC-MMORF exhibited slightly higher energy in the subcortical area (Fig. 7F), suggesting higher image sharpness near the cortex in the T_1w template built with the proposed method and slightly higher image sharpness in the subcortical area in the T_1w template built with MC-MMORF. Visual inspection of FA maps of the DTI templates constructed by the different methods showed that white matter features near the cortex were better delineated in the template constructed using the proposed method (Fig. 8A). The standard deviation of the FA template generated by the proposed method was lower than that of other methods (Fig. 8B). Near the cortex, FA image sharpness in the template built with the proposed method was similar to or higher than that of other templates (Fig. 8C), while in the subcortical area FA image sharpness was higher in the template built with MC-MMORF (Fig. 8E). FA values were higher in a relatively higher number of white matter voxels throughout

the brain in the templates constructed by MC-MMORF, followed by the proposed method, compared to other methods ($p<10^{-10}$) (Fig. 8D,F). The contours of white matter obtained for the different template construction methods by thresholding the corresponding white matter tissue probability maps were overlaid on the corresponding FA maps and visual inspection showed good alignment of white matter information across T_1 w and DTI templates for all methods (Appendix).

The performance of T_1 w and DTI templates when used as references for spatial normalization of data from Dataset 2 was compared across multimodal template construction methods. In terms of the T_1 w intra-modality inter-subject spatial normalization precision, the template constructed with the proposed method allowed higher average pairwise JI of gray matter masks from Dataset 2 in the cerebral cortex, and similar but still higher average pairwise JI in cerebellar cortex compared to the other methods ($p<0.05$), indicating higher inter-subject T_1 w spatial normalization precision especially in the cerebral cortex when using the template of the proposed method as reference (Fig. 9). The template constructed using MC-MMORF allowed higher average pairwise JI of gray matter masks in the subcortical gray matter ($p<0.05$), indicating higher spatial normalization precision in subcortical gray matter when using the MC-MMORF template as reference (Fig. 9). In terms of the DTI intra-modality inter-subject spatial normalization precision for Dataset 2, the template constructed with the proposed method resulted in a higher number of white matter voxels with lower DTED near the cortex ($p<10^{-3}$) (Fig. 10A), and similar but still higher number of white matter voxels with lower DTED in the subcortical area ($p<0.01$) (Fig. 10B) compared to templates constructed with the other methods, suggesting higher inter-subject DTI spatial normalization precision for Dataset 2 especially near the cortex when using the DTI template of the proposed method as reference. Lastly, the T_1 w and DTI templates of the proposed method allowed the highest inter-modality spatial matching of gray matter and cerebrospinal fluid masks from Dataset 2, and the MC-MMORF templates allowed the highest inter-modality spatial matching of white matter masks from Dataset 2, as shown by the higher average JI between masks of Dataset 2 that experienced T_1 w-based transformations and those that experienced tensor-based transformations ($p<0.05$) (Fig. 11).

4. Discussion

The present work (A) introduced an iterative method for multimodal T_1 w and DTI template construction, (B) used this method to develop T_1 w and DTI templates of the older adult brain in a common space, and (C) evaluated the performance of the method across iterations and compared it to the performance of state-of-the-art approaches based on multichannel registration. It was demonstrated that more iterations of the proposed method enhanced the characteristics of the resulting T_1 w and DTI templates as well as the spatial matching between these templates. The templates of the older adult brain generated by the final iteration of the proposed method provided better delineation of brain structures, higher discriminability between tissues, and higher image sharpness near the cortex compared to templates generated with approaches that employ multichannel registration. In addition, the spatial matching between the T_1 w and DTI templates constructed by the proposed method approximated the template alignment achieved with methods employing multichannel registration. Finally, when using the templates generated

by the proposed method as references for spatial normalization of older adult T_1w and DTI data from the independent Dataset 2, both the intra-modality inter-subject normalization precision and the inter-modality spatial matching were higher in most evaluations than those achieved with templates constructed with other methods. Overall, the present work brought new insights into multimodal template construction, generated much-needed high quality T_1w and DTI templates of the older adult brain in a common space (available for download at www.nitrc.org/projects/miitra; version 1.5), and conducted a thorough, quantitative evaluation of available multimodal template construction methods.

4.1. Evaluation of the proposed method across iterations

The quality of the T_1w and DTI templates as well as the spatial matching between these templates was shown to improve with more iterations of the proposed method and appeared to stabilize at 4 iterations. These findings were because spatial matching among data used in template construction (Dataset 1) also improved across iterations. Alternating between T_1w-driven and DTI-driven spatial normalization during template construction may have allowed the two modalities to work synergistically in reducing misregistrations. It has been shown that T_1w-based registration using most currently available tools introduces high frequency deformation in the white matter where T_1w images have low contrast (Lange et al., 2020a). Subsequent DTI-based registration may address this limitation in white matter and in neighboring structures. In addition, T_1w-based registration may help improve spatial matching near the cortex and at tissue interfaces where DTI data may have less contrast. Thus, alternating between T_1w-driven and DTI-driven spatial normalization in the proposed method may have improved spatial matching among data used in template construction and thereby improved the quality of the T_1w and DTI templates. The spatial matching between T_1w and DTI templates also improved with more iterations. Even though in the final iteration of the proposed method the DTI data experience one additional transformation that is not applied to the T_1w data, multiple iterations where the two modalities work synergistically to find a common space and all transformations are applied to data from both modalities not only improved spatial matching among data used in template construction, but also gradually increased the alignment of the resulting T_1w and DTI templates.

4.2. Comparison of the proposed method to other multimodal template construction methods

The final T_1w and DTI templates generated with the proposed method exhibited overall higher image quality, especially near the cortex, than those constructed using methods based on multichannel registration and the same raw data. This was probably due to more precise intra-modality spatial matching of data from individual participants (Dataset 1) when using single channel instead of multichannel registration. Multichannel registration aims at optimizing inter-subject spatial matching for all modalities, but due to the very different contrast in T_1w and DTI data, T_1w information may be distracting when attempting to optimize inter-subject matching of DTI features, and the opposite. Therefore, multichannel registration may have resulted in less precise spatial matching of the features of interest in each modality compared to considering each modality separately, thereby compromising

the quality of both templates. The proposed method overcomes this limitation by aiming at maximizing inter-subject spatial matching for each modality separately.

Among all evaluations of template quality, the proposed method was slightly outperformed only in the following two. In the subcortical area, the T_1w template built with MC-MMORF exhibited slightly higher discriminability between gray matter and cerebrospinal fluid than other templates. This may be because MMORF produces fewer local volume changes and shape distortions within subcortical white matter compared to ANTs registration (Lange et al., 2020a). However, probably due to the same reason, the caudolenticular gray bridges which are fine structures in the subcortical area were not visible in the T_1w template of MC-MMORF and were only visible with the proposed method (Fig. 7A). Also in the subcortical area, the FA map of the DTI template constructed by MC-MMORF exhibited higher image sharpness than other templates. This was probably due to the higher FA values in white matter of the MC-MMORF template, which in turn might be due to log-Euclidean averaging of diffusion tensors used by MC-MMORF (Lange et al., 2020b; Roumazeilles et al., 2021; https://git.fmrib.ox.ac.uk/cart/mm-template-construction). Previous studies have suggested that the log-Euclidean metric (Arsigny et al., 2006) leads to a substantial bias especially for high FA tensors, and thus the FA values in the MC-MMORF template might be overestimated (Pasternak et al., 2010, 2012).

Visual inspection demonstrated that all template construction methods provided equally good alignment between T_1w and DTI templates. Quantitatively, methods based on multichannel registration achieve excellent alignment of T_1w and DTI templates by default because the same transformations are applied to data from both modalities during template construction. The proposed method also applies the same transformations to data from both modalities up until the final step of the final iteration, at which point the DTI data experience one additional transformation that is not applied to the T_1w data. Yet, it was shown that the last iteration of the proposed method (iteration 4) achieved Jaccard indices between the white matter masks and between the gray matter masks of T_1w and DTI templates of approximately 0.97 and 0.95 respectively, while methods based on multichannel registration had a Jaccard index of 1 by default. The above suggests that the proposed method provides higher quality templates at the cost of only a slight (not noticeable) mismatch between the two templates.

When used as a reference for spatial normalization of data from the independent Dataset 2, the T_1w template generated with the proposed method allowed higher intra-modality inter-subject spatial normalization precision in the cerebral and cerebellar cortices. The DTI template of the proposed method also allowed higher overall intra-modality inter-subject spatial normalization precision compared to DTI templates constructed with other methods. Furthermore, inter-modality spatial matching in gray matter and in CSF was the highest when using the T_1w and DTI templates of the proposed method. These findings were primarily due to the enhanced image quality of the templates constructed with the proposed method. Sharper templates preserving fine details and allowing better delineation of brain structures have been shown to provide higher spatial normalization precision, and this has a direct impact on the sensitivity and specificity of template-based neuroimaging studies (Hsu et al., 2015; Ridwan et al., 2021; Zhang and Arfanakis, 2018). The MC-MMORF

T_1 w template allowed higher intra-modality inter-subject spatial normalization precision only in the subcortical gray matter, and highest inter-modality matching in the white matter, possibly due to the limited shape deformations in the subcortical area when using MMORF.

4.3. Caveats

In addition to the multiple strengths of the proposed multimodal T_1 w and DTI template construction method and the analysis presented above, this work also has a few limitations. The proposed template construction method is more computationally intensive and time consuming compared to other approaches. However, this limitation is not of concern since standardized templates are constructed once and used in multiple studies, and therefore the cost in computational resources and processing time associated with the proposed method is unimportant. In addition, the present work employed state-of-the-art image registration and template construction methods and data of typical quality from older adults in the 65–95 years age-range. Future work should also consider other registration algorithms as well as data with different image quality and from different age-ranges. It is not possible to explore all combinations here, but we believe our choice to use state-of-the-art methods and data of typical quality is scientifically justified and of highest interest. Additionally, the focus of the present work was multimodal T_1 w and DTI templates. Developing templates for other pairs of modalities e.g. T_2 w and DTI, or extending the proposed method to more than two modalities, constitute interesting research questions requiring extensive investigation that is beyond the scope of this work. Finally, we recently presented a method for constructing a T_1 w template of the older adult brain with submillimeter resolution and showed that, compared to 1 mm T_1 w templates, the high-resolution template provided higher inter-subject spatial normalization precision and enabled detection of smaller inter-group morphometric differences for older adult data (Niaz et al., 2022). Therefore, studies requiring only a T_1 w template may benefit from using the previously constructed high-resolution template compared to the 1 mm template constructed here (note that the two templates are also located in a slightly different space). In future work, we will incorporate the method we presented in Niaz et al., 2022, to develop multimodal T_1 w and DTI templates at submillimeter resolution.

4.4. Adapting the proposed method for registration of an individual's T_1 w and DTI data to the templates generated in this work

The iterative approach for multimodal T_1 w and DTI template construction can be adapted for registration of T_1 w and DTI data from individual older adults to the templates constructed in this work. The approach is similar to that described in Section 2.3 with the difference that there is no group-wise normalization, no weighted averaging of signals, and no template building or updating, since data from a single individual are registered to standardized templates. More specifically, in step 1, T_1 w data of an individual older adult are registered to the T_1 w MIITRA template and the resulting transformation is also applied to the DTI data of the individual (assuming the T_1 w and DTI data of the individual are originally in the same space). In step 2, DTI data of the same individual older adult are registered to the DTI MIITRA template and the resulting transformation is also applied to the T_1 w data of the individual. Steps 1 and 2 are then repeated for multiple iterations, and the transformations from all steps and iterations are combined so

that each image is interpolated only once throughout the whole process. A script named reg_to_MIITRA_T1_and_DTI.sh that executes this iterative registration of an individual's T_1 w and DTI data to the templates constructed in this work is available for download at www.nitrc.org/projects/miitra.

5. Conclusion

The present work introduced an iterative method for multimodal T_1 w and DTI template construction and generated templates of the older adult brain that were shown to provide better delineation of brain structures, higher discriminability between tissues, and higher image sharpness near the cortex compared to templates generated with state-of-the-art approaches based on multichannel registration. Furthermore, the spatial matching between the T_1 w and DTI templates constructed by the proposed method approximated the template alignment achieved by default with methods employing multichannel registration. The higher image quality of the templates generated by the proposed method facilitated higher precision of intra-modality inter-subject normalization of an independent older adult dataset as well as higher inter-modality spatial matching, which are well-known to directly impact the sensitivity and specificity of template-based neuroimaging studies. Overall, the present work brought new insights into multimodal template construction and generated much-needed high quality T_1 w and DTI templates of the older adult brain in a common space (available for download as part of the MIITRA atlas at www.nitrc.org/projects/miitra; version 1.5).

Supplementary Material

Refer to Web version on PubMed Central for supplementary material.

Acknowledgements

The authors would like to thank the participants and staff of the Rush University Memory and Aging Project and Alzheimer's Disease Neuroimaging Initiative.

Funding

This study was supported by National Institutes of Health grants R01AG052200, P30AG010161, R01AG17917, P30AG072975, and R01AG015819.

In addition, part of the data collection and sharing for this project was funded by the Alzheimer's Disease Neuroimaging Initiative (ADNI) (National Institutes of Health Grant U01 AG024904) and DOD ADNI (Department of Defense award number W81XWH-12–2–0012). ADNI is funded by the National Institute on Aging, the National Institute of Biomedical Imaging and Bioengineering, and generous contributions from the following: AbbVie; Alzheimer's Association; Alzheimer's Drug Discovery Foundation; Araclon Biotech; BioClinica, Inc.; Biogen; Bristol-Myers Squibb Company; CereSpir, Inc.; Cogstate; Eisai; Elan Pharmaceuticals, Inc.; Eli Lilly and Company; EuroImmun; F. Hoffmann-La Roche and its affiliated company Genentech, Inc.; Fujirebio; GE Healthcare; IXICO Ltd.; Janssen Alzheimer Immunotherapy Research & Development, LLC.; Johnson & Johnson Pharmaceutical Research & Development LLC.; Lumosity; Lundbeck; Merck & Co., Inc.; Meso Scale Diagnostics, LLC.; NeuroRx Research; Neurotrack Technologies; Novartis Pharmaceuticals Corporation; Pfizer Inc.; Piramal Imaging; Servier; Takeda Pharmaceutical Company; and Transition Therapeutics. The Canadian Institutes of Health Research is providing funds to support ADNI clinical sites in Canada. Private sector contributions are facilitated by the Foundation for the National Institutes of Health (www.fnih.org/). The grantee organization is the Northern California Institute for Research and Education, and the study is coordinated by the Alzheimer's Therapeutic Research Institute at the University of Southern California. ADNI data are disseminated by the Laboratory for Neuro Imaging at the University of Southern California.

Data and template availability statement

The data used in this work can be assessed by submitting a request to www.radc.rush.edu. All templates are available for download at www.nitrc.org/projects/miitra (version 1.5).

References

Alexander DC, Gee JC, 2000. Elastic matching of diffusion tensor images. Comput. Vision Image Understand 77 (2), 233–250.

Arsigny V, Fillard P, Pennec X, Ayache N, 2006. Log Euclidean metrics for fast and simple calculus on diffusion tensors. Magn. Reson. Med 56, 411–421. [PubMed: 16788917]

Arthofer C, Smith SM, Jenkinson M, Andersson J, Lange F, 2021. Multimodal MRI template construction from UK Biobank: oxford-MM-0. Presented at the Organisation for Human Brain Mapping (OHBM).

Avants B, Duda JT, Kim J, Zhang H, Pluta J, Gee JC, Whyte J, 2008a. Multivariate analysis of structural and diffusion imaging in traumatic brain injury. Acad. Radiol 15 (11), 1360–1375. doi:10.1016/j.acra.2008.07.007. [PubMed: 18995188]

Avants BB, Cook PA, Ungar L, Gee JC, Grossman M, 2010a. Dementia induces correlated reductions in white matter integrity and cortical thickness: a multivariate neuroimaging study with sparse canonical correlation analysis. Neuroimage 50 (3), 1004–1016. [PubMed: 20083207]

Avants BB, Epstein CL, Grossman M, Gee JC, 2008b. Symmetric diffeomorphic image registration with cross-correlation: evaluating automated labeling of elderly and neurodegenerative brain. Med. Image Anal 12 (1), 26–41. [PubMed: 17659998]

Avants BB, Tustison NJ, Song G, 2009. Advanced normalization tools (ANTS). Insight J. 2 (365), 1–35. Retrieved from https://www.insight-journal.org/browse/publication/681 .

Avants BB, Tustison NJ, Song G, Cook PA, Klein A, Gee JC, 2011. A reproducible evaluation of ANTs similarity metric performance in brain image registration. Neuroimage 54 (3), 2033–2044. [PubMed: 20851191]

Avants BB, Yushkevich P, Pluta J, Minkoff D, Korczykowski M, Detre J, Gee JC, 2010b. The optimal template effect in hippocampus studies of diseased populations. Neuroimage 49 (3), 2457–2466. [PubMed: 19818860]

Bennett DA, Buchman AS, Boyle PA, Barnes LL, Wilson RS, Schneider JA, 2018. Religious orders study and rush memory and aging project. J. Alzheimer's Dis 64 (s1), S161–S189. [PubMed: 29865057]

Blatter DD, Bigler ED, Gale SD, Johnson SC, Anderson CV, Burnett BM, Parker N, Kurth S, Horn SD, 1995. Quantitative volumetric analysis of brain MR: normative database spanning 5 decades of life. AJNR Am. J. Neuroradiol 16 (2), 241–251. [PubMed: 7726068]

Cabeen RP, Bastin ME, Laidlaw DH, 2017. A Comparative evaluation of voxel-based spatial mapping in diffusion tensor imaging. Neuroimage 146, 100–112. [PubMed: 27847347]

Chang L-C, Jones DK, Pierpaoli C, 2005. RESTORE: robust estimation of tensors by outlier rejection. Magnet. Resonance Med 53 (5), 1088–1095.

Chang L-C, Walker L, Pierpaoli C, 2012. Informed RESTORE: a method for robust estimation of diffusion tensor from low redundancy datasets in the presence of physiological noise artifacts. Magnet. Resonance Med 68 (5), 1654–1663.

Courchesne E, Chisum HJ, Townsend J, Cowles A, Covington J, Egaas B, Harwood M, Hinds S, Press GA, 2000. Normal brain development and aging: quantitative analysis at in vivo MR imaging in healthy volunteers. Radiology 216 (3), 672–682. [PubMed: 10966694]

Dickie DA, Karama S, Ritchie SJ, Cox SR, Sakka E, Royle NA, Aribisala BS, Hernández MV, Maniega SM, Pattie A, Corley J, Starr JM, Bastin ME, Evans AC, Deary IJ, Wardlaw JM, 2016. Progression of white matter disease and cortical thinning are not related in older community-dwelling subjects. Stroke 47 (2), 410–416. [PubMed: 26696646]

Doshi J, Erus G, Ou Y, Gaonkar B, Davatzikos C, 2013. Multi-atlas skull-stripping. Acad. Radiol 20 (12), 1566–1576. [PubMed: 24200484]

Duda RO, Hart PE, Stork DG, 2012. Pattern Classification. John Wiley and Sons.

Farokhian F, Beheshti I, Sone D, Matsuda H, 2017. Comparing CAT12 and VBM8 for detecting brain morphological abnormalities in temporal lobe epilepsy. Front. Neurol 10.3389/fneur.2017.00428/full.

Ferreira JR, Oliveira MC, Freitas AL, 2014. Performance Evaluation of Medical Image Similarity Analysis in a Heterogeneous Architecture. In: 2014 IEEE 27th International Symposium on Computer-Based Medical Systems, pp. 159–164.

Fischl B, 2012. FreeSurfer. Neuroimage 62 (2), 774–781. [PubMed: 22248573]

Fonov V, Evans AC, Botteron K, Almli CR, McKinstry RC, Collins DL, 2011. Unbiased average age-appropriate atlases for pediatric studies. Neuroimage 54 (1), 313–327. [PubMed: 20656036]

Ge Y, Grossman RI, Babb JS, Rabin ML, Mannon LJ, Kolson DL, 2002. Age-related total gray matter and white matter changes in normal adult brain. Part I: volumetric MR imaging analysis. AJNR Am. J. Neuroradiol 23 (8), 1327–1333. [PubMed: 12223373]

Good CD, Johnsrude IS, Ashburner J, Henson RN, Friston KJ, Frackowiak RS, 2001. A voxel-based morphometric study of ageing in 465 normal adult human brains. Neuroimage 14 (1 Pt 1), 21–36. [PubMed: 11525331]

Guimond A, Guttmann CRG, Warfield SK, Westin C, 2002. Deformable registration of DT-MRI data based on transformation invariant tensor characteristics. In: Proceedings IEEE International Symposium on Biomedical Imaging, pp. 761–764.

Heckemann RA, Ledig C, Gray KR, Aljabar P, Rueckert D, Hajnal JV, Hammers A, 2015. Correction: brain extraction using label propagation and group agreement: pincram. PLoS One 10 (8), e0135746. [PubMed: 26267800]

Hsu Y-C, Lo Y-C, Chen Y-J, Wedeen VJ, Isaac Tseng W-Y, 2015. NTU-D-SI-122: a diffusion spectrum imaging template with high anatomical matching to the ICBM-152 space: a DSI Template in the ICBM-152 Space. Hum. Brain Mapp 36 (9), 3528–3541. [PubMed: 26095830]

Irfanoglu MO, Nayak A, Jenkins J, Hutchinson EB, Sadeghi N, Thomas CP, Pierpaoli C, 2016. DR-TAMAS: diffeomorphic registration for tensor accurate alignment of anatomical structures. Neuroimage 132, 439–454. [PubMed: 26931817]

Irfanoglu MO, Nayak A, Jenkins J, Pierpaoli C, 2017. TORTOISE v3: improvements and new features of the NIH diffusion MRI processing pipeline. In: Proceedings of the 25th Annual Meeting of ISMRM Presented at the International Society for Magnetic Resonance in Medicine.

Jörsäter S, 1993. Methods in astronomical image processing with special applications to the reduction of CCD data. Central Activity in Galaxies. Lecture Notes in Physics, 413 Sandqvist A, Ray TP. Springer, Berlin, Heidelberg doi:10.1007/3-540-56371-7_24.

Joshi S, Davis B, Jomier M, Gerig G, 2004. Unbiased diffeomorphic atlas construction for computational anatomy. Neuroimage 23 (Suppl 1), S151–S160. [PubMed: 15501084]

Keihaninejad S, Ryan NS, Malone IB, Modat M, Cash D, Ridgway GR, Zhang H, Fox NC, Ourselin S, 2012. The importance of group-wise registration in tract based spatial statistics study of neurodegeneration: a simulation study in Alzheimer's disease. PLoS One 7 (11), e45996. [PubMed: 23139736]

Kim S-G, Jung WH, Kim SN, Jang JH, Kwon JS, 2015. Alterations of gray and white matter networks in patients with obsessive-compulsive disorder: a multimodal fusion analysis of structural MRI and DTI using mCCA+jICA. PLoS One 10 (6), e0127118. [PubMed: 26038825]

Klein A, Andersson J, Ardekani BA, Ashburner J, Avants B, Chiang M-C, Christensen GE, Collins DL, Gee J, Hellier P, Song JH, Jenkinson M, Lepage C, Rueckert D, Thompson P, Vercauteren T, Woods RP, Mann JJ, Parsey RV, 2009. Evaluation of 14 nonlinear deformation algorithms applied to human brain MRI registration. Neuroimage 46 (3), 786–802. [PubMed: 19195496]

Kochunov P, Thompson PM, Lancaster JL, Bartzokis G, Smith S, Coyle T, Royall DR, Laird A, Fox PT, 2007. Relationship between white matter fractional anisotropy and other indices of cerebral health in normal aging: tract-based spatial statistics study of aging. Neuroimage 35 (2), 478–487. [PubMed: 17292629]

Lalys F, Haegelen C, Ferre JC, El-Ganaoui O, Jannin P, 2010. Construction and assessment of a 3-T MRI brain template. Neuroimage 49, 345–354. doi:10.1016/j.neuroimage.2009.08.007. [PubMed: 19682582]

Lange FJ, Ashburner J, Smith SM, Andersson JLR, 2020a. A symmetric prior for the regularisation of elastic deformations: improved anatomical plausibility in nonlinear image registration. Neuroimage 219, 116962. doi:10.1016/j.neuroimage.2020.116962. [PubMed: 32497785]

Lange FJ, Smith SM, Bertelsen MF, Khrapichev AA, Manger PR, Mars RB, Andersson JLR, 2020b. Multimodal MRI template creation in the ring-tailed lemur and rhesus macaque. Biomedical Image Registration. WBIR 2020. Lecture Notes in Computer Science, 12120 špiclin Ž, McClelland J, Kybic J, Goksel O. Springer, Cham doi:10.1007/978-3-030-50120-4_14.

Liu RSN, Lemieux L, Bell GS, Sisodiya SM, Shorvon SD, Sander JWAS, Duncan JS, 2003. A longitudinal study of brain morphometrics using quantitative magnetic resonance imaging and difference image analysis. Neuroimage 20 (1), 22–33. [PubMed: 14527567]

Li Y, Verma R, 2011. Multichannel image registration by feature-based information fusion. IEEE Trans. Med. Imaging 30 (3), 707–720. [PubMed: 21097379]

Madden DJ, Whiting WL, Huettel SA, White LE, MacFall JR, Provenzale JM, 2004. Diffusion tensor imaging of adult age differences in cerebral white matter: relation to response time. Neuroimage 21 (3), 1174–1181. [PubMed: 15006684]

Mazziotta JC, Toga AW, Evans A, Fox P, Lancaster J, 1995. A probabilistic atlas of the human brain: theory and rationale for its development. The International Consortium for Brain Mapping (ICBM). Neuroimage 2 (2), 89–101. doi:10.1006/nimg.1995.1012. [PubMed: 9343592]

Mazziotta J, Toga A, Evans A, Fox P, Lancaster J, Zilles K, … Mazoyer B, 2001. A probabilistic atlas and reference system for the human brain: international consortium for brain mapping (ICBM). Philos. Trans. R. Soc. Lond., B, Biol. Sci 356 (1412), 1293–1322. doi:10.1098/rstb.2001.0915. [PubMed: 11545704]

McCarthy CS, Ramprashad A, Thompson C, Botti J-A, Coman IL, Kates WR, 2015. A comparison of FreeSurfer-generated data with and without manual intervention. Front. Neurosci 9, 379. [PubMed: 26539075]

Misaki M, Savitz J, Zotev V, Phillips R, Yuan H, Young KD, Drevets WC, Bodurka J, 2015. Contrast enhancement by combining T1- and T2-weighted structural brain MR Images: contrast Enhancement with T1w and T2w MRI. Magnet. Resonance Med 74 (6), 1609–1620.

Mori S, Oishi K, Jiang H, Jiang L, Li X, Akhter K, Hua K, Faria AV, Mahmood A, Woods R, Toga AW, Pike GB, Neto PR, Evans A, Zhang J, Huang H, Miller MI, van Zijl P, Mazziotta J, 2008. Stereotaxic white matter atlas based on diffusion tensor imaging in an ICBM template. Neuroimage 40 (2), 570–582. [PubMed: 18255316]

Niaz MR, Ridwan AR, Wu Y, Alzheimer's Disease Neuroimaging Initiative, Bennett DA, Arfanakis K, 2022. Development and evaluation of a high resolution 0.5 mm isotropic T1-weighted template of the older adult brain. Neuroimage 248, 118869. doi:10.1016/j.neuroimage.2021.118869. [PubMed: 34986396]

Park H-J, Kubicki M, Shenton ME, Guimond A, McCarley RW, Maier SE, Kikinis R, Jolesz FA, Westin C-F, 2003. Spatial normalization of diffusion tensor MRI using multiple channels. Neuroimage 20 (4), 1995–2009. [PubMed: 14683705]

Pasternak O, Sochen N, Basser PJ, 2010. The effect of metric selection on the analysis of diffusion tensor MRI data. Neuroimage 49 (3), 2190–2204. doi:10.1016/j.neuroimage.2009.10.071. [PubMed: 19879947]

Pasternak O, Sochen N, Basser PJ, 2012. Metric selection and diffusion tensor swelling. In: New Developments in the Visualization and Processing of Tensor Fields, Part of the Series Mathematics and Visualization. Springer-Verlag, Berlin Heidelber, pp. 323–336.

Peng H, Orlichenko A, Dawe RJ, Agam G, Zhang S, Arfanakis K, 2009. Development of a human brain diffusion tensor template. Neuroimage 46 (4), 967–980. doi:10.1016/j.neuroimage.2009.03.046. [PubMed: 19341801]

Pfefferbaum A, Sullivan EV, 2003. Increased brain white matter diffusivity in normal adult aging: relationship to anisotropy and partial voluming. Magn. Reson. Med 49 (5), 953–961. doi:10.1002/mrm.10452. [PubMed: 12704779]

Pierpaoli C, Walker L, Irfanoglu MO, Barnett A, Basser P, Chang LC, Koay C, Pajevic S, Rohde G, Sarlls J, 2010. TORTOISE: an integrated software package for processing of diffusion MRI data. ISMRM 18th Annual Meeting, 1597.

Ridwan AR, Niaz MR, Wu Y, Qi X, Zhang S, Kontzialis M, Javierre-Petit C, Tazwar M, Alzheimer's Disease Neuroimaging Initiative, Bennett DA, Yang Y, Arfanakis K, 2021. Development and evaluation of a high performance T1-weighted brain template for use in studies on older adults. Hum. Brain Mapp 42 (6), 1758–1776. doi:10.1002/hbm.25327. [PubMed: 33449398]

Rohde GK, Barnett AS, Basser PJ, Marenco S, Pierpaoli C, 2004. Comprehensive approach for correction of motion and distortion in diffusion-weighted MRI. Magnet. Resonance Med 51 (1), 103–114.

Rohlfing T, Zahr NM, Sullivan EV, Pfefferbaum A, 2010. The SRI24 multichannel atlas of normal adult human brain structure. Hum. Brain Mapp 31 (5), 798–819. [PubMed: 20017133]

Rohlfing T, Kroenke CD, Sullivan EV, Dubach MF, Bowden DM, Grant KA, Pfefferbaum A, 2012. The INIA19 template and NeuroMaps atlas for primate brain image parcellation and spatial normalization. Front. Neuroinform 6, 27. doi:10.3389/fninf.2012.00027. [PubMed: 23230398]

Roumazeilles L, Lange FJ, Benn RA, Andersson J, Bertelsen MF, Manger PR, Flach E, Khrapitchev AA, Bryant KL, Sallet J, Mars RB, 2021. Cortical morphology and white matter tractography of three phylogenetically distant primates: evidence for a simian elaboration. Cereb. Cortex doi:10.1093/cercor/bhab285, bhab285. Advance online publication.

Salat DH, Tuch DS, Greve DN, van der Kouwe AJW, Hevelone ND, Zaleta AK, Rosen BR, Fischl B, Corkin S, Rosas HD, Dale AM, 2005. Age-related alterations in white matter microstructure measured by diffusion tensor imaging. Neurobiol. Aging 26 (8), 1215–1227. [PubMed: 15917106]

Sasamoto A, Miyata J, Kubota M, Hirao K, Kawada R, Fujimoto S, Tanaka Y, Hazama M, Sugihara G, Sawamoto N, Fukuyama H, Takahashi H, Murai T, 2014. Global association between cortical thinning and white matter integrity reduction in schizophrenia. Schizophr Bull. 40 (2), 420–427. [PubMed: 23461997]

Scahill RI, Frost C, Jenkins R, Whitwell JL, Rossor MN, Fox NC, 2003. A longitudinal study of brain volume changes in normal aging using serial registered magnetic resonance imaging. Arch. Neurol 60 (7), 989–994. [PubMed: 12873856]

Senjem ML, Gunter JL, Shiung MM, Petersen RC, Jack CR Jr., 2005. Comparison of different methodological implementations of voxel-based morphometry in neurodegenerative disease. Neuroimage 26 (2), 600–608. [PubMed: 15907317]

Smith CD, Chebrolu H, Wekstein DR, Schmitt FA, Markesbery WR, 2007. Age and gender effects on human brain anatomy: a voxel-based morphometric study in healthy elderly. Neurobiol. Aging 28 (7), 1075–1087. [PubMed: 16774798]

Smith SM, Jenkinson M, Johansen-Berg H, Rueckert D, Nichols TE, Mackay CE, Watkins KE, Ciccarelli O, Cader MZ, Matthews PM, Behrens TEJ, 2006. Tract-based spatial statistics: voxelwise analysis of multi-subject diffusion data. Neuroimage 31 (4), 1487–1505. [PubMed: 16624579]

Sullivan EV, Adalsteinsson E, Pfefferbaum A, 2006. Selective age-related degradation of anterior callosal fiber bundles quantified in vivo with fiber tracking. Cereb. Cortex 16 (7), 1030–1039. [PubMed: 16207932]

Sullivan EV, Rohlfing T, Pfefferbaum A, 2010. Quantitative fiber tracking of lateral and interhemispheric white matter systems in normal aging: relations to timed performance. Neurobiol. Aging 31 (3), 464–481. [PubMed: 18495300]

Sydykova D, Stahl R, Dietrich O, Ewers M, Reiser MF, Schoenberg SO, Möller H-J, Hampel H, Teipel SJ, 2007. Fiber connections between the cerebral cortex and the corpus callosum in Alzheimer's disease: a diffusion tensor imaging and voxel-based morphometry study. Cereb. Cortex 17 (10), 2276–2282. [PubMed: 17164468]

Toga AW, Thompson PM, Mori S, Amunts K, Zilles K, 2006. Towards multimodal atlases of the human brain. Nat. Rev. Neurosci 7 (12), 952–966. [PubMed: 17115077]

Tustison NJ, Avants BB, Cook PA, Zheng Y, Egan A, Yushkevich PA, Gee JC, 2010. N4ITK: improved N3 bias correction. IEEE Trans. Med. Imaging 29 (6), 1310–1320. [PubMed: 20378467]

Van Hecke W, Leemans A, Sage CA, Emsell L, Veraart J, Sijbers J, Sunaert S, Parizel PM, 2011. The effect of template selection on diffusion tensor voxel-based analysis results. Neuroimage 55 (2), 566–573. [PubMed: 21146617]

Wang Y, Xu M, Geng L, Zhao Y, Guo Z, Fan Y, Niu Y, 2021. DTI atlases evaluations. Neuroinformatics 1–25. doi:10.1007/s12021-021-09521-y. [PubMed: 32728882]

Wang Z, Bovik AC, Sheikh HR, Simoncelli EP, 2004. Image quality assessment: from error visibility to structural similarity. IEEE Trans. Image Process 13 (4), 600–612. [PubMed: 15376593]

Yang G, Zhou S, Bozek J, Dong H-M, Han M, Zuo X-N, Liu H, Gao J-H, 2020. Sample sizes and population differences in brain template construction. Neuroimage 206, 116318. [PubMed: 31689538]

Yoon U, Fonov VS, Perusse D, Evans AC, 2009. The effect of template choice on morphometric analysis of pediatric brain data. Neuroimage 45 (3), 769–777. [PubMed: 19167509]

Zhang H, Avants BB, Yushkevich PA, Woo JH, Wang S, McCluskey LF, Elman LB, Melhem ER, Gee JC, 2007. High-dimensional spatial normalization of diffusion tensor images improves the detection of white matter differences: an example study using amyotrophic lateral sclerosis. IEEE Trans. Med. Imaging 26 (11), 1585–1597. doi:10.1109/TMI.2007.906784. [PubMed: 18041273]

Zhang S, Arfanakis K, 2018. Evaluation of standardized and study-specific diffusion tensor imaging templates of the adult human brain: template characteristics, spatial normalization accuracy, and detection of small inter-group FA differences. Neuroimage 172, 40–50. doi:10.1016/j.neuroimage.2018.01.046. [PubMed: 29414497]

Zhang S, Peng H, Dawe RJ, Arfanakis K, 2011. Enhanced ICBM diffusion tensor template of the human brain. Neuroimage 54 (2), 974–984. [PubMed: 20851772]

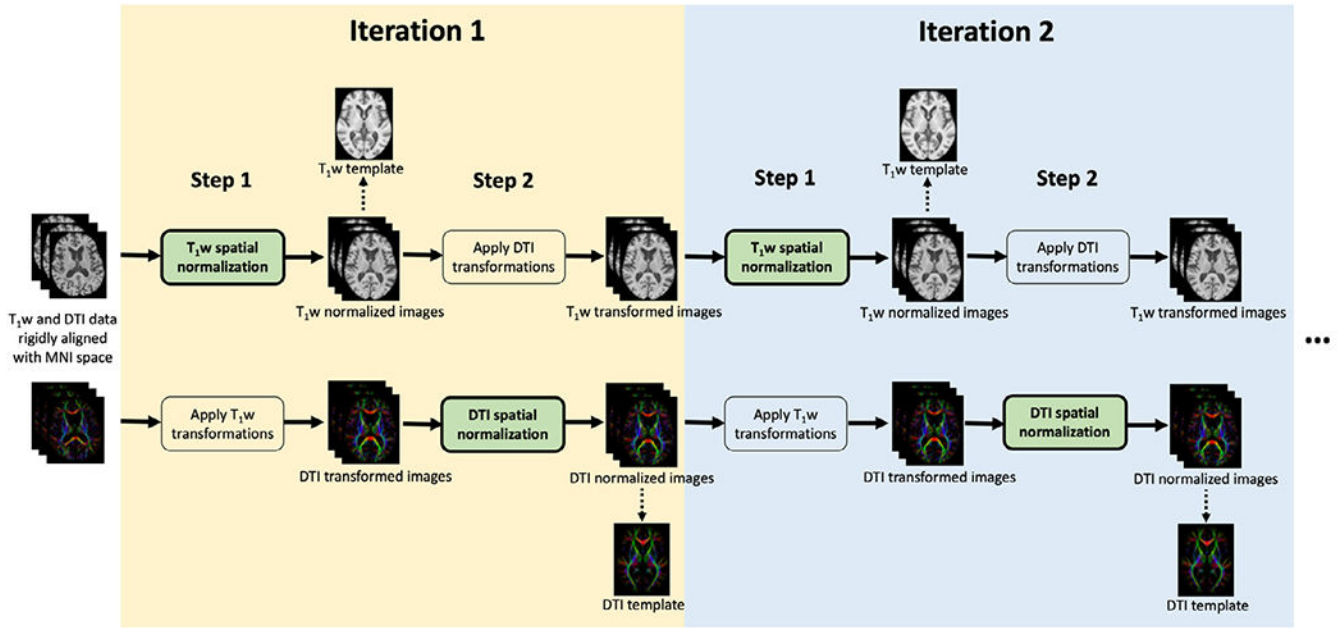

Fig. 1.

Schematic representation of the proposed method for construction of multimodal T_1 w and DTI templates.

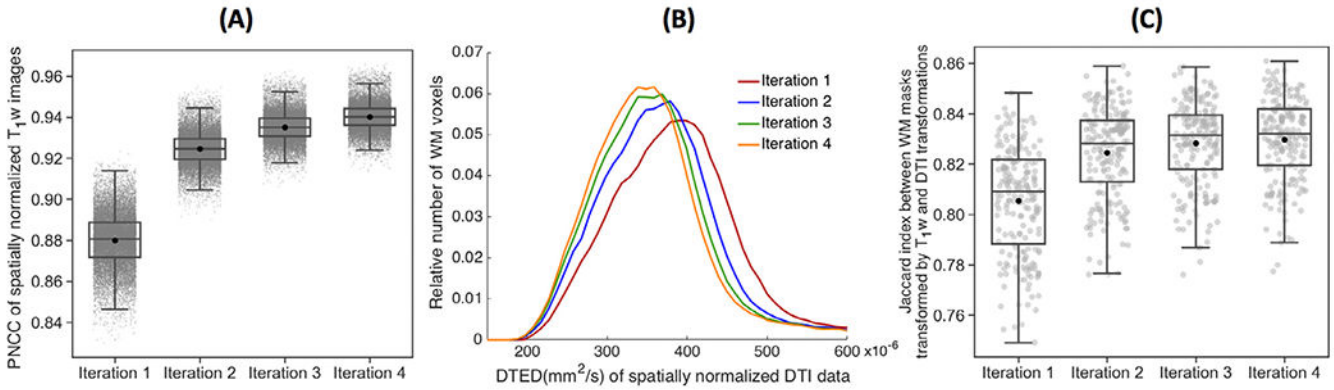

Fig. 2.

(A) Boxplots of the pairwise normalized cross-correlation (PNCC) of spatially normalized T_1 w images used in the construction of the T_1 w template, at different iterations of the proposed method. (B) Histograms of the relative number of white matter voxels at different values of the average pairwise Euclidean distance of tensors (DTED) across spatially normalized DTI data used in the construction of the DTI template, for different iterations of the proposed method. (C) Boxplots of the Jaccard index (JI) between white matter masks transformed by T_1 w and DTI transformations over all data used in template construction, at different iterations of the proposed method.

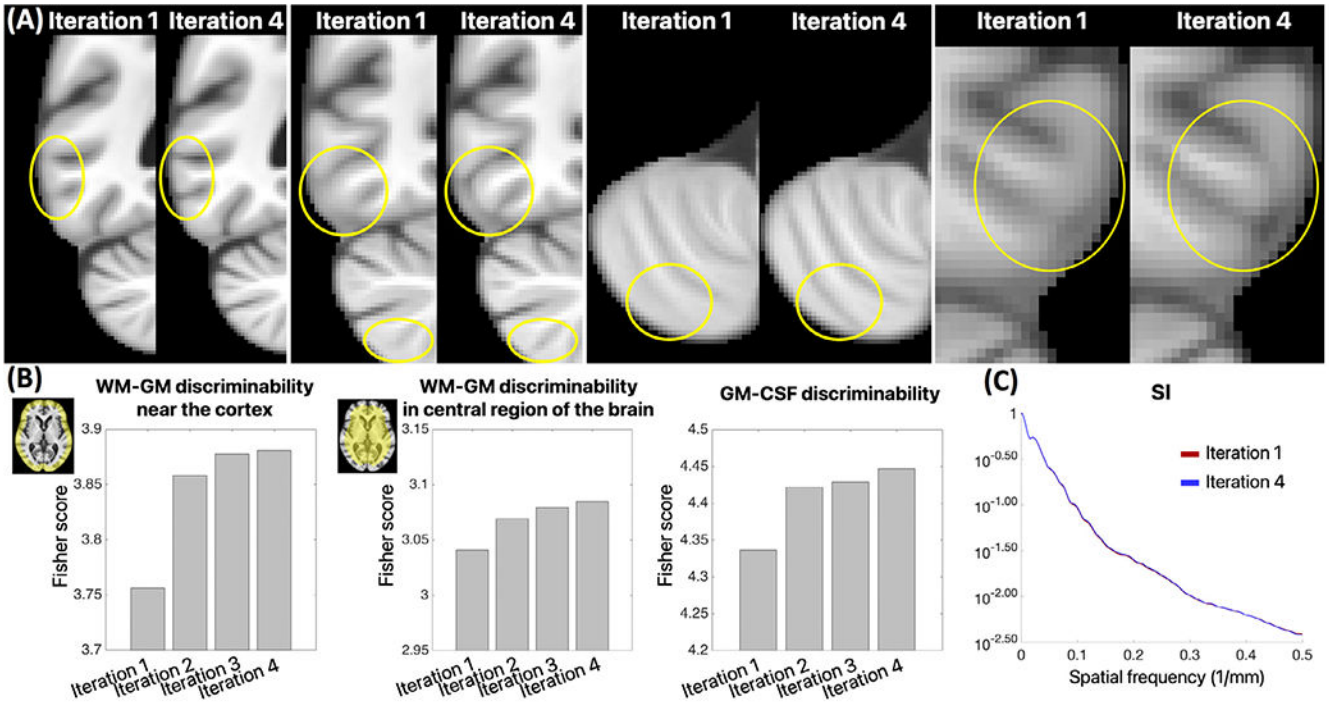

Fig. 3.

(A) Magnified portions of the T_1 w templates generated in iterations 1 and 4. (B) Discriminability (Fisher score) between tissues in T_1 w templates generated at different iterations. The brain regions under consideration are highlighted in yellow in the inset axial images. (C) Normalized power spectra of T_1 w templates for the superior-inferior (SI) axis and iterations 1 and 4.

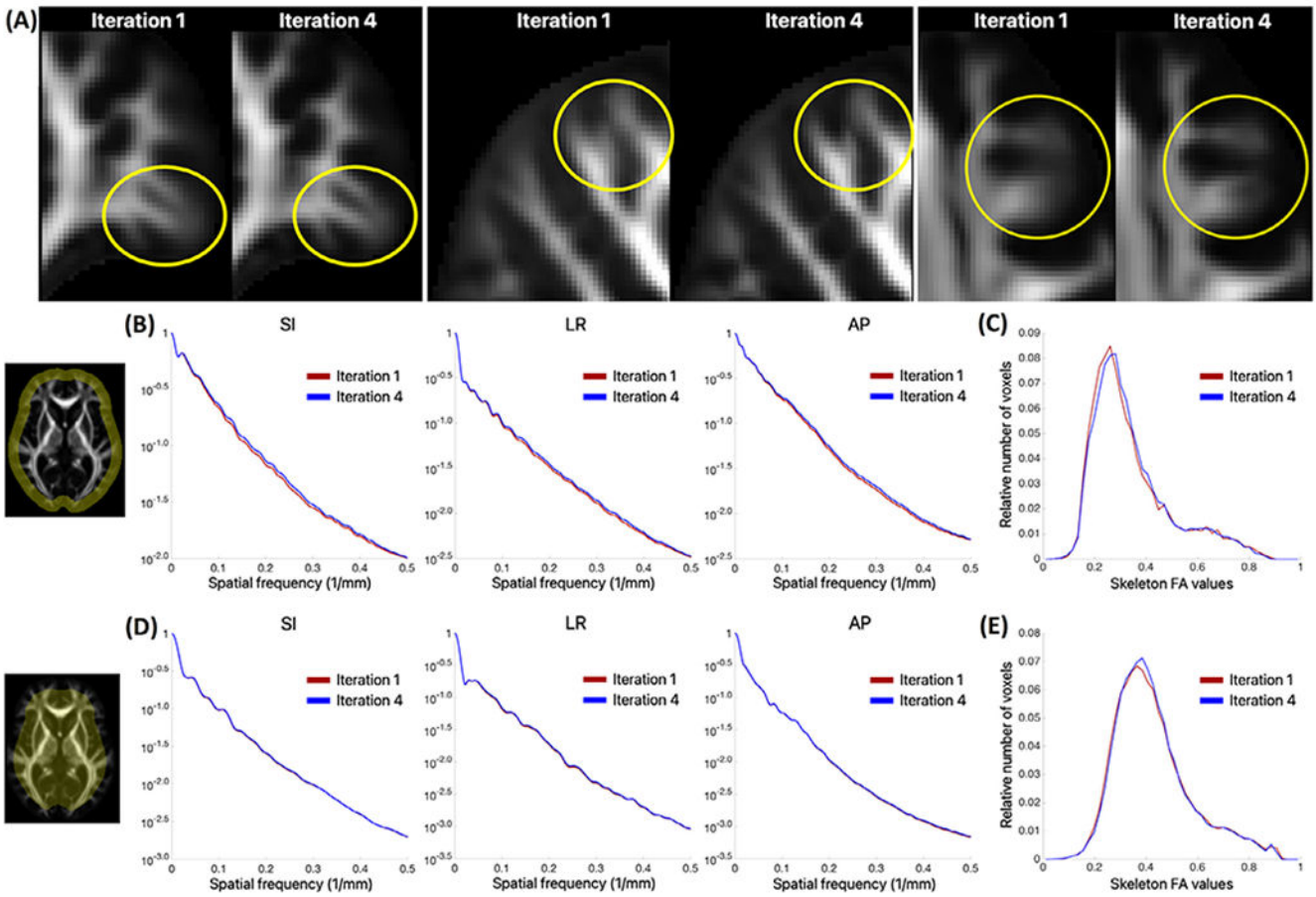

Fig. 4.

(A) Magnified portions of FA maps from the DTI templates generated in iterations 1 and 4. Normalized power spectra of FA maps for the superior-inferior (SI), left-right (LR) and anterior-posterior (AP) axes near the cortex (B) and in the subcortical area of the brain (D) for iterations 1 and 4. Histograms of template FA values in the white matter near the cortex (C) and in the subcortical area of the brain (E) for iterations 1 and 4.

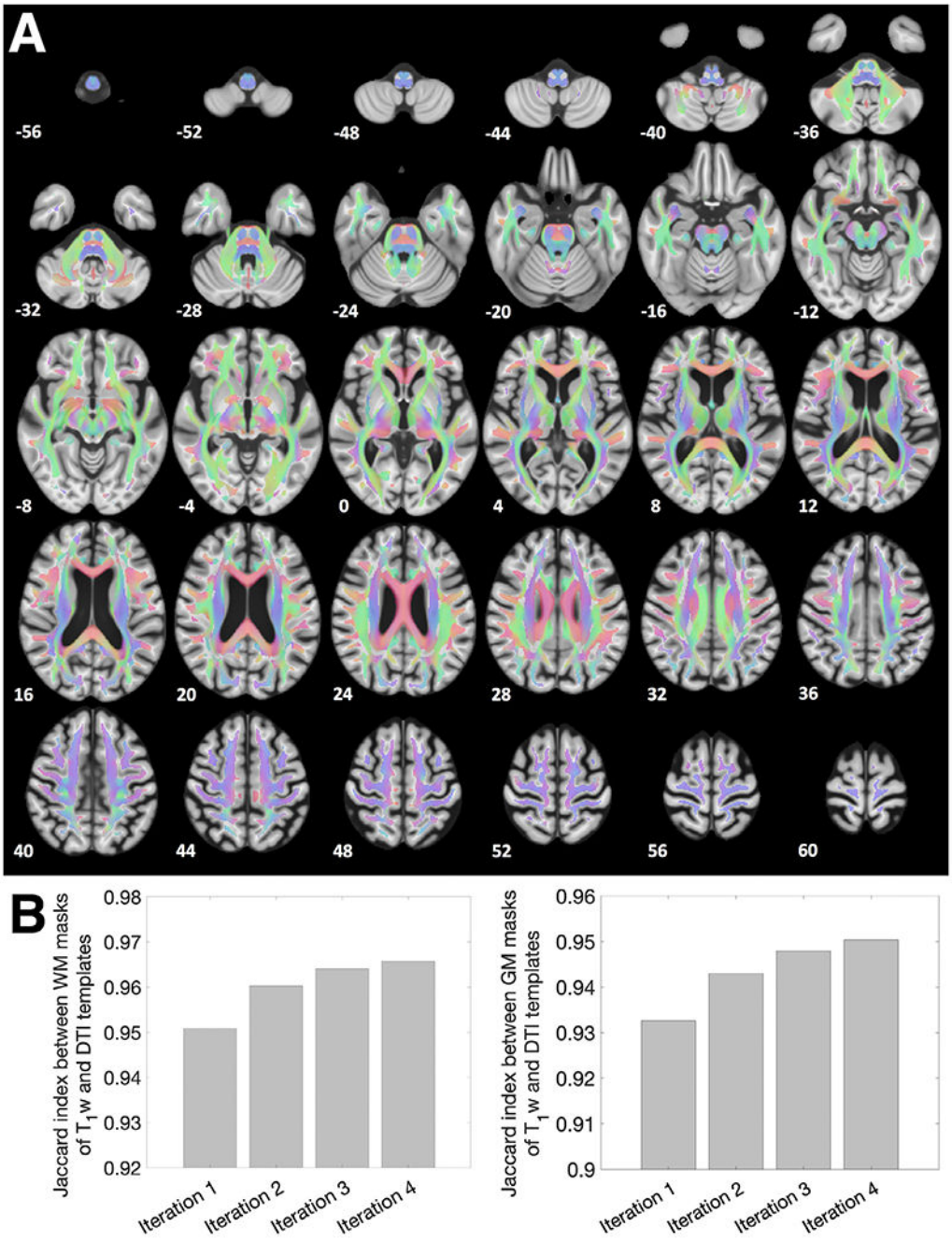

Fig. 5.

(A) Axial views of FA colormaps generated with the proposed method in iteration 4 overlaid on the corresponding T_1 w template. (B) Jaccard index between white matter (WM) masks and between gray matter (GM) masks of the T_1 w and DTI templates generated in different iterations.

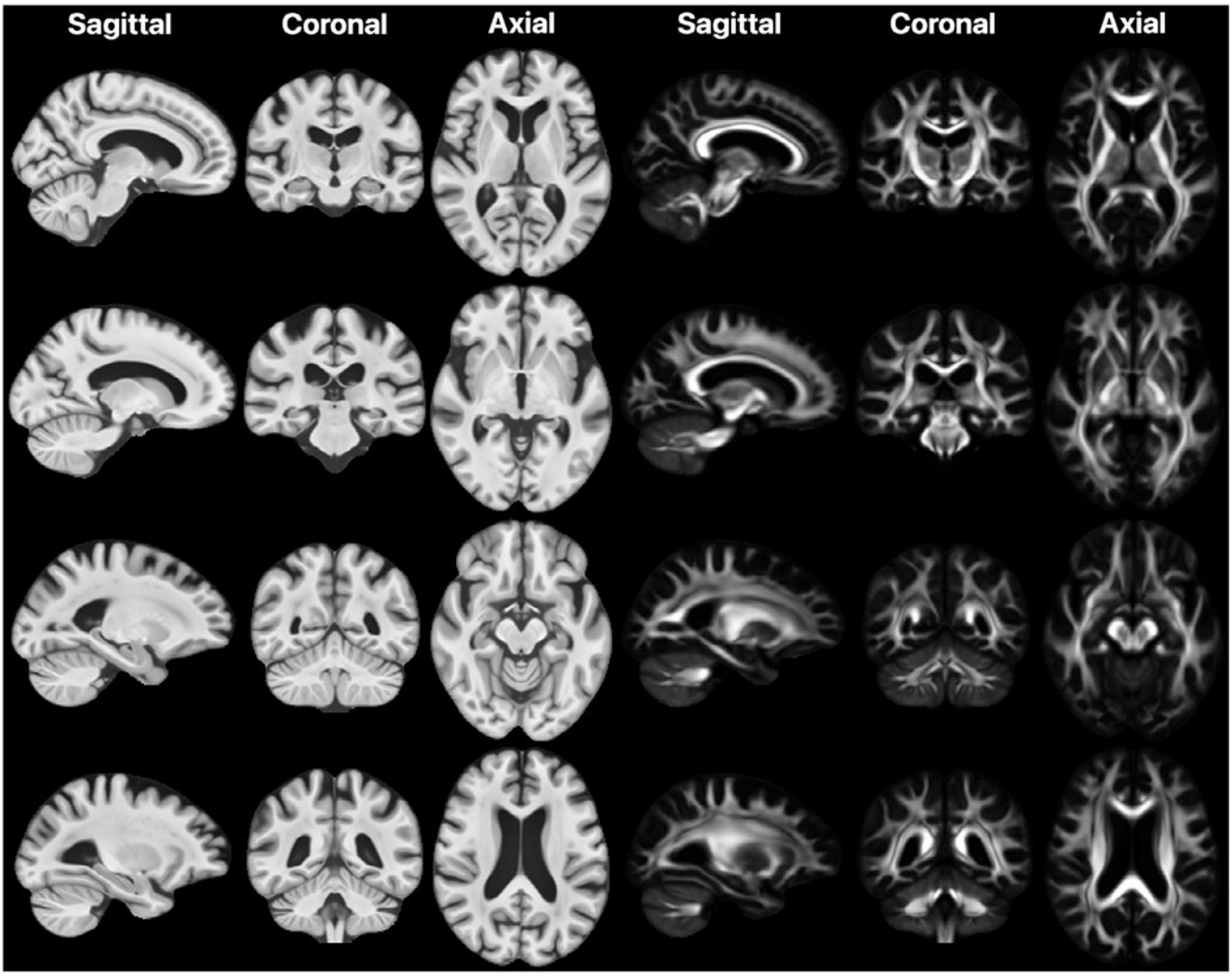

Fig. 6.

Examples of sagittal, coronal and axial slices of the final T_1 w template and the FA map of the final DTI template generated with the proposed method.

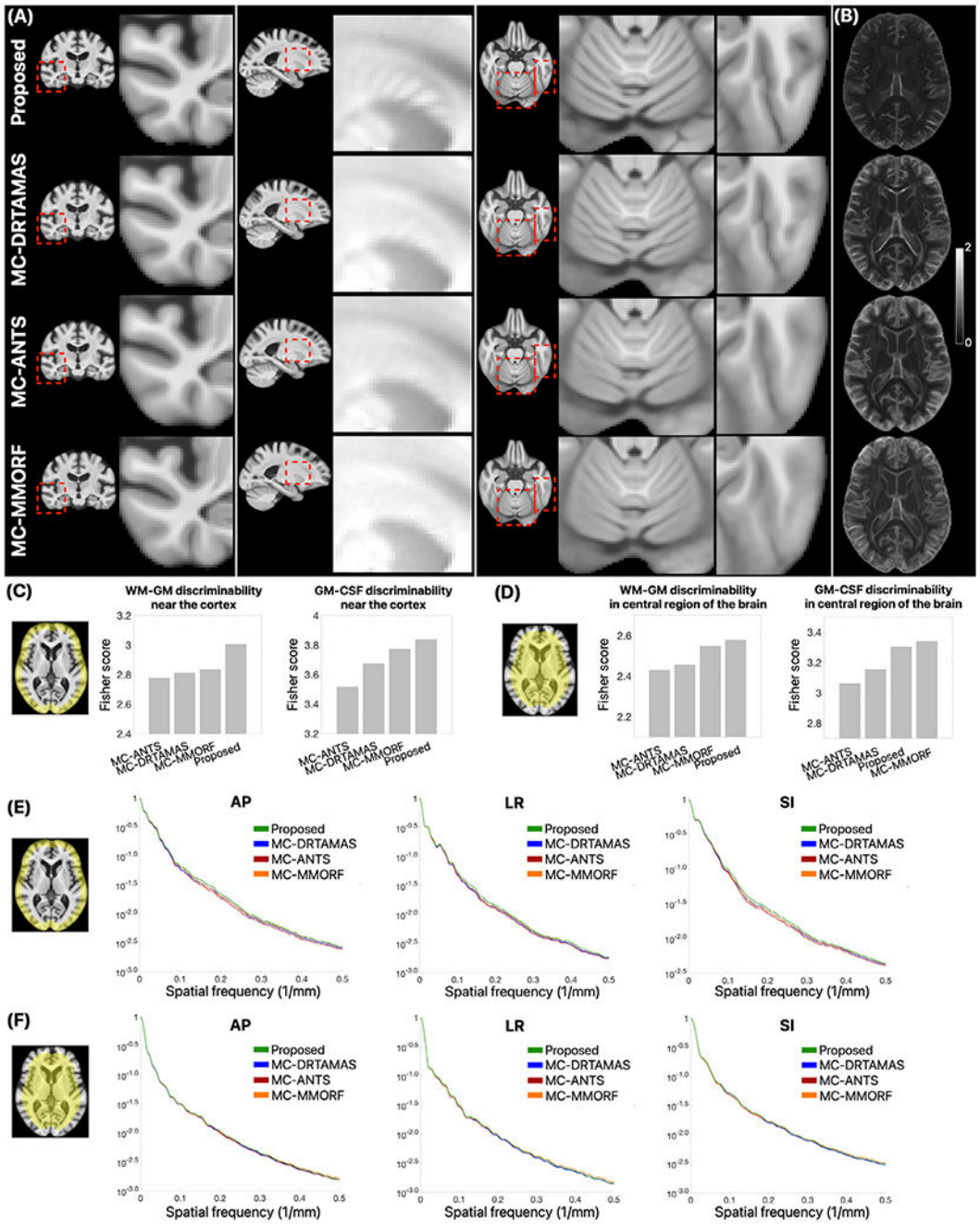

Fig. 7.

(A) Comparison of the T_1 w templates generated with different methods. (B) Maps of standard deviation across the spatially normalized T_1 w images used to construct the different templates. (C, D) Fisher score between tissues for the different T_1 w templates, near the cortex (C) and in the subcortical area of the brain (D). (E, F) Normalized power spectra of the different T_1 w templates for the anterior-posterior (AP), left-right (LR) and superior-inferior (SI) axes near the cortex (E) and in the subcortical area of the brain (F).

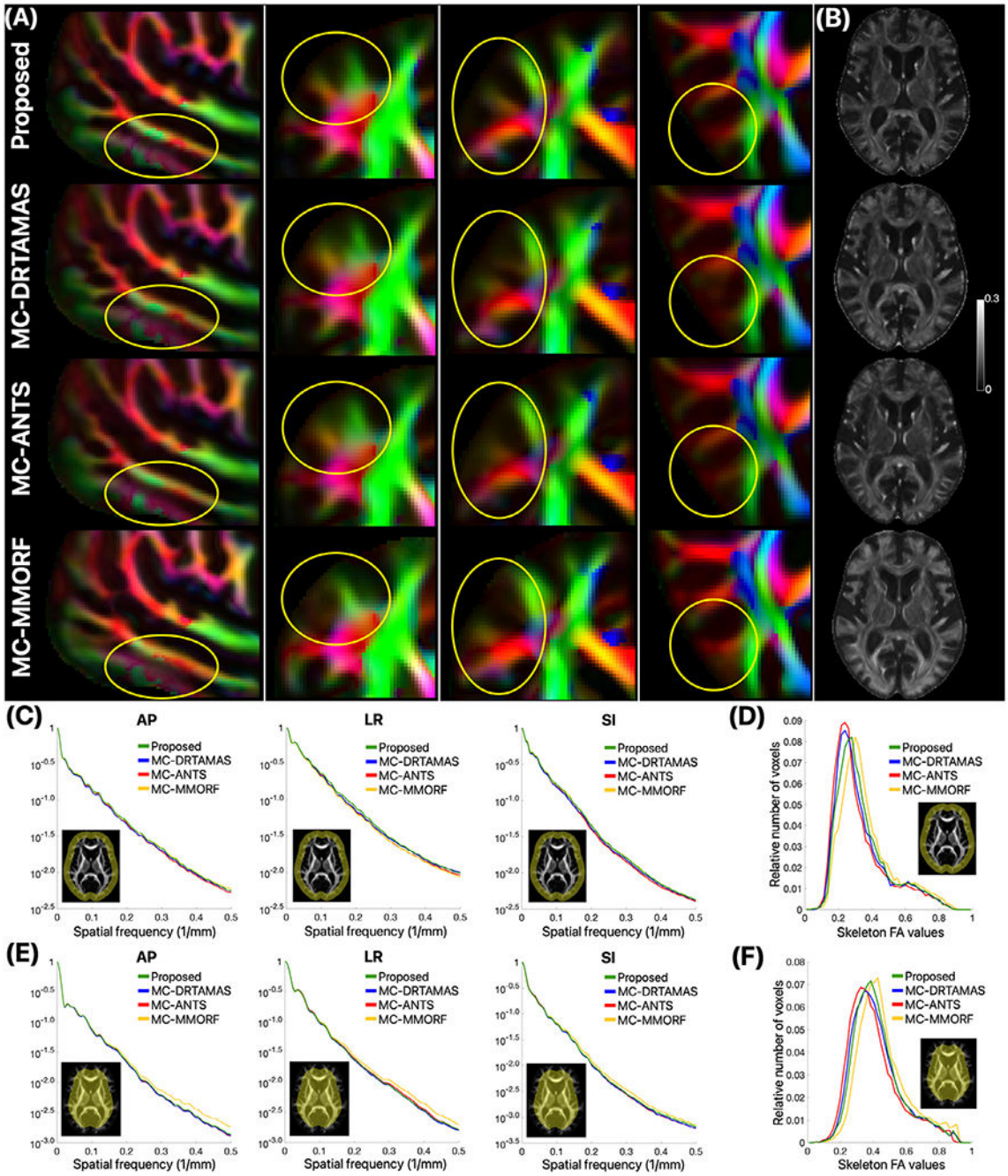

Fig. 8.

(A) Comparison of FA colormaps from the DTI templates generated with the different methods. (B) Maps of standard deviation across the spatially normalized FA maps of the datasets used to construct the different DTI templates. Normalized power spectra of FA maps of the different DTI templates for the superior-inferior (SI), left-right (LR) and anterior-posterior (AP) axes near the cortex (C) and in the subcortical area of the brain (E). Histograms of template FA values in the white matter near the cortex (D) and in the subcortical area of the brain (F) for the different DTI templates.

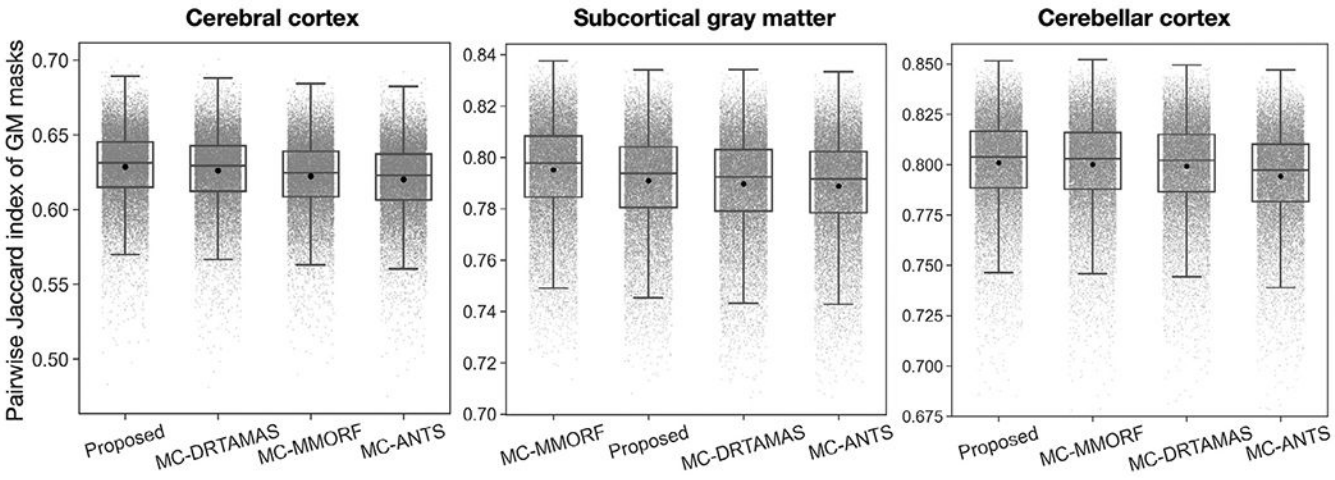

Fig. 9.

Boxplots of the pairwise Jaccard index (PJI) of gray matter masks in the cerebral cortex (left), subcortical gray matter (middle), and cerebellar cortex (right) from spatially normalized T_1 w data of Dataset 2 when using different T_1 w templates as references.

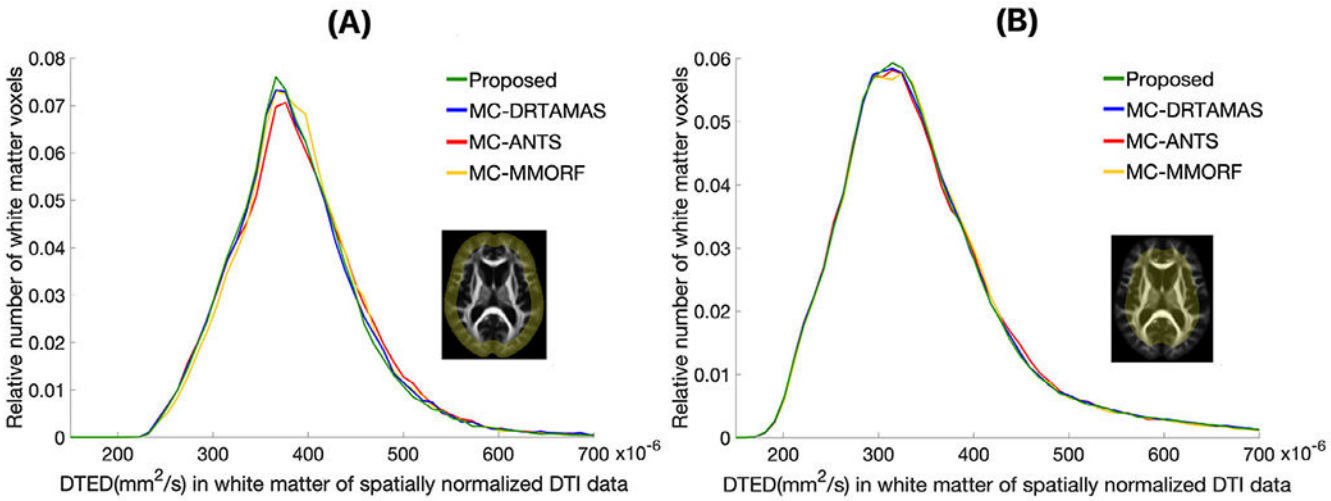

Fig. 10.

Histograms of the relative number of white matter voxels at different values of the average pairwise Euclidean distance of tensors (DTED) across spatially normalized DTI data from Dataset 2, near the cortex (A), and in the subcortical area of the brain (B), when using different DTI templates as references.

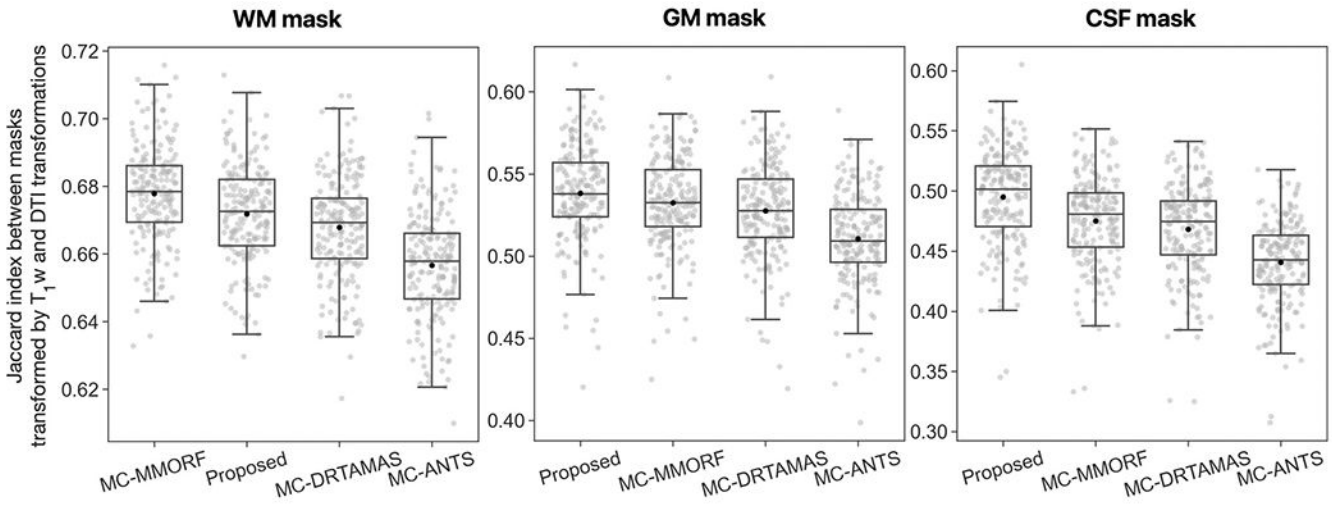

Fig. 11.

Boxplots of the Jaccard index (JI) between white matter masks (left), gray matter masks (middle), and cerebrospinal fluid masks (right) of Dataset 2 transformed by T_1w and DTI transformations when using the templates constructed by the different methods as references for spatial normalization.